On the zero-point energy of elliptic-cylindrical and spheroidal boundaries

A thesis presented in partial
fulfilment of the requirements
for the degree of

Doctor of Philosophy
in Theoretical Physics

at Massey University
New Zealand

Adrian Robert Kitson

2009

Abstract

Zero-point energy is the energy of the vacuum. Disturbing the vacuum results in a change in the zero-point energy. In 1948, Casimir considered the change in the zero-point energy when the vacuum is disturbed by two parallel metal plates. The plates disturb the vacuum by restricting the quantum fluctuations of the electromagnetic field. Casimir found that the change in the zero-point energy implies that the plates are attracted to each other. With the recent advances made in the experimental verification of this remarkable result, theoretical interest has been rekindled. In addition to the original parallel plate configuration, several other boundaries have been studied. In this thesis, two novel boundaries are considered: elliptic-cylindrical and spheroidal. The results for these boundaries lead to the conjecture that zero-point energy does not change for small deformations of the boundary that preserve volume. Assuming the conjecture, it is shown that zero-point energy plays a stabilizing role in quantum chromodynamics, the leading theory of the strong interaction.

Acknowledgments

I would like to thank my supervisor Tony Signal for suggesting the topic, giving me the freedom to explore, but always being there when I needed help. Tony, without your support and patience when times were hard, this thesis simply would not exist. Thank you!

The work on elliptical cylinders was done in collaboration with August Romeo, whom I sincerely thank.

Special thanks go to Kim Milton and Bruce van Brunt for helping me more than they probably realize.

The figures of lattice simulations in the chapter on quantum chromodynamics are used with kind permission from Derek Leinweber.

Massey University, the Institute of Fundamental Sciences and the Royal Society of New Zealand are all gratefully acknowledged for financial assistance.

Perhaps I should have included my dad in the previous list? But, dad, I hope you know you mean more to me than just helping pay the bills! To the rest of my family: thank you for listening to me go on about maths and physics... and pretending to be interested.

Finally, I would like to thank all my friends, especially Bill, Warwick, G and Clare.

I dedicate this thesis to my daughter, Delta.

Table of contents

List of figures

Nomenclature

In this thesis, Dirac's constant $\hbar$ and the speed of light c are both unity. The signature of the Minkowski metric is taken to be $(1,-1,-1,-1)$.

Chapter 1

Introduction

Zero-point energy is the energy of the vacuum. If the vacuum is disturbed, then consequently there is a change in the zero-point energy. In 1948, Casimir considered the disturbance when two parallel metal plates are placed in the vacuum [1]. He found the change in the zero-point energy per unit transverse area to be

$$\mathscr{E} = -\frac{\pi^2}{720a^3}, \tag{1.1}$$

where a is the separation between the plates. Figure 1.1 shows a plot of Casimir's result. Because the energy monotonically decreases as the separation between the plates decreases, the plates are mutually attracted to each other. This attractive force has not only been observed qualitatively, but also experimentally verified quantitatively.

Given the small size of the force, which is of the order of millipascals for separations of the order of microns, and the challenge in maintaining parallel plates, it is not surprising that the early experiments were rather unsuccessful. In 1958, Sparnaay confirmed the presence of the force but could not verify its dependence on the separation between the plates [2]. Much better success has been achieved in the last decade. Measuring the related force between a plate and a sphere, theory and experiment now agree spectacularly well [3–5]. The plate and sphere arrangement makes alignment much simpler. The zero-point energy is related to the zero-point energy of parallel plates by the proximity force theorem [6], which is reasonably accurate providing that the radius of the sphere is much greater than the separation between the plate and the sphere. The theoretical result is also modified to account for finite conductivity, nonzero temperature and surface roughness. Recently, the parallel plate arrangement

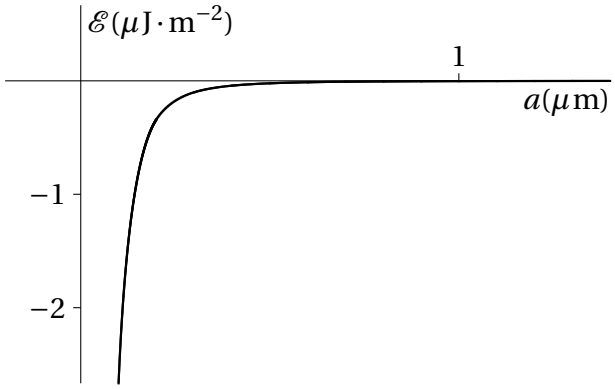

Figure 1.1: Casimir's result for the zero-point energy of parallel plates.

was considered again [7]. For further information regarding the experimental verification of Casimir's result, and zero-point energy in general, see the 2001 review by Bordag, Mohideen and Mostepanenko [8]. More up-to-date results can be found in the 2005 report by Lamoreaux [9].

Casimir obtained his result by modeling the plates with perfectly-conducting boundary conditions on parallel planes. The boundary conditions affect the quantum fluctuations of the electromagnetic field and consequently the zero-point energy. However, some authors argue that such ideal boundary conditions are unphysical; for example, the charge on the electron does not appear in Casimir's result (1.1). An alternative approach is to model the plates with an external field, one that strongly couples to the electromagnetic field and that is sharply concentrated on the plates. This field-theoretical approach has been studied by Bordag *et al.* [10, 11], and again by Graham *et al.* [12–14]. In addition to recovering Casimir's result in the appropriate limit, the field-theoretical approach offers an insight into the dependence of the zero-point energy on the coupling and, therefore, the physical properties of the plates. However, the field-theoretical approach is not followed in this thesis; Casimir's approach is followed. The main reason is that only ideal boundaries are considered, for which the field-theoretical approach offers no advantage.

Zero-point energy is not restricted to the situation considered by Casimir. Several

generalizations have been considered. Some generalizations, such as finite conductivity and nonzero temperature [15], are important in the experimental verification of Casimir's result. Other generalizations, such as massless and massive scalar, spinor and colour fields [16–18], other dimensions [19–21], and dynamical boundaries [22], are of theoretical interest. For more information on these and other generalizations, see the 2001 monograph by Milton [23].

A particularly interesting generalization, and the main focus of this thesis, is the geometry of the boundary. Only a handful of boundaries have been studied because calculating zero-point energy requires solving the field equation analytically, and this can only be done for certain boundaries that are highly symmetrical. Examples include wedges [24], cuboidal boxes and rectangular cylinders [19]; however, the three boundaries that have received the most attention are parallel planes and spherical and cylindrical boundaries.

In 1956, motivated by his result for parallel planes, Casimir proposed that zero-point energy might play a stabilizing role in the Abraham-Lorentz model of the electron [25]. In the Abraham-Lorentz model, the charge on the electron is evenly distributed over the boundary of a sphere of radius R. An attractive force is required to balance the Coulombic repulsion. The change in the zero-point energy for a spherical boundary was calculated by Boyer in 1968 [26]. Surprisingly, the result implies a repulsive force, invalidating Casimir's proposal. The result has been confirmed by many authors [27–30],

$$E = \frac{0.04617\ldots}{R}, \tag{1.2}$$

where R is the radius of the sphere.

The cylindrical boundary was first studied by DeRaad and Milton in 1981 [31]. They calculated the change in the zero-point energy per unit longitudinal length to be

$$\mathscr{E} = -\frac{0.01356\ldots}{R^2}, \tag{1.3}$$

where R is the radius of the cylinder. DeRaad and Milton's result implies an attractive

force.

From the results for parallel planes and spherical and cylindrical boundaries, it is clear that zero-point energy is highly dependent on the boundary. It follows that studying new boundaries is useful in understanding zero-point energy. In this thesis two novel boundaries are studied: elliptic-cylindrical and spheroidal.

An elliptic cylinder is a cylinder whose cross-section is an ellipse. The ellipticity of an elliptic cylinder is measured in terms of eccentricity, which ranges from zero to one. When the eccentricity is zero, the elliptical cylinder is a circular cylinder. In the limit as eccentricity tends to one, the elliptical cylinder becomes parallel planes.

Spheroids come in two varieties: prolate and oblate. Prolate spheroids are formed by rotating an ellipse about its major axis; oblate spheroids are formed by rotating an ellipse about its minor axis. Depending on the eccentricity, the limiting cases of a prolate spheroid are a sphere and a circular cylinder; the limiting cases of an oblate spheroid are a sphere and parallel planes.

While it is possible to write down an expression for the zero-point energy of an arbitrary boundary [28], evaluating this expression can be impossible. In this thesis the zero-point energy of the elliptic-cylindrical and spheroidal boundaries is evaluated in terms of a formal series in terms of small eccentricity. Formal series allow operations such as differentiation and integration to be performed term-wise. There is, however, no guarantee that the results will converge for all eccentricity. In fact, the results may only hold asymptotically as eccentricity tends to zero. Nevertheless, using formal series is a well-established mathematical technique, similar to perturbation theory.

This thesis is arranged as follows. In chapter 2 the different methods used to calculate zero-point energy are discussed. Particular attention is paid to the Green-function and zeta-function methods, which are the main methods used in this thesis. Several detailed examples are included. The elliptic-cylindrical boundary is considered in chapter 3. Then in chapter 4 the spheroidal boundary is considered. The spheroidal boundary is continued in chapter 5, where it is considered together with quantum

chromodynamics. Concluding remarks are made in chapter 6. Finally, an appendix is included on the special functions associated with elliptic-cylindrical and spheroidal boundaries.

Chapter 2

Zero-point energy

2.1 Introduction

The main methods used in this thesis to calculate zero-point energy are the Green-function and the zeta-function methods. The purpose of this chapter is to introduce these methods. The chapter concludes with two detailed examples. These examples not only illustrate how each method is used in practice, but also form the foundation on which later results are built. First, zero-point energy is formally defined.

2.2 Formal definition

The zero-point energy of a quantum field is given by the expectation value of the Hamiltonian operator H with respect to the vacuum state $|0\rangle$; that is, $\langle 0|H|0\rangle$. Suppose that the vacuum is disturbed by the presence of some boundary ∂V. Let $\langle 0|H|0\rangle_{\partial V}$ denote the zero-point energy of the disturbed vacuum and $\langle 0|H|0\rangle_0$ denote the zero-point energy of an equal volume of the undisturbed vacuum. The change in the zero-point energy is formally given by

$$E = \langle 0|H|0\rangle_{\partial V} - \langle 0|H|0\rangle_0 . \tag{2.1}$$

Expression (2.1) is not well-defined; in fact, it is indeterminate. This is now shown for a massless real scalar field ϕ; the analysis for other fields is similar [32].

Consider the Lagrangian density for the scalar field

$$\mathscr{L} = \frac{1}{2}\partial_\mu\phi\,\partial^\mu\phi\,. \tag{2.2}$$

Applying the Euler-Lagrange equation,

$$\frac{\partial\mathscr{L}}{\partial\phi} - \partial_\mu\frac{\partial\mathscr{L}}{\partial(\partial_\mu\phi)} = 0\,, \tag{2.3}$$

yields the Klein-Gordon field equation

$$\partial_\mu\partial^\mu\phi = 0\,. \tag{2.4}$$

The Hamiltonian density is given by

$$\mathscr{H} = \pi\partial_0\phi - \mathscr{L}\,, \tag{2.5}$$

where $\pi = \partial_0\phi$ is the conjugate momentum field. Using the field equation (2.4), the Hamiltonian density can also be given by

$$\mathscr{H} = \frac{1}{2}\left(\partial_0\phi\,\partial^0\phi - \phi\,\partial_0\partial^0\phi\right) + \frac{1}{2}\nabla\cdot(\phi\nabla\phi)\,. \tag{2.6}$$

The Hamiltonian H for a region V is the integral of the Hamiltonian density over that region. Using Gauss's theorem,

$$H = \frac{1}{2}\int_V d^3x\left(\partial_0\phi\,\partial^0\phi - \phi\,\partial_0\partial^0\phi\right) + \frac{1}{2}\int_{\partial V} dS\,\phi\,\mathbf{n}\cdot\nabla\phi\,, \tag{2.7}$$

where $\mathbf{n}$ is the outward unit normal to the boundary ∂V.

The analysis so far has been for a classical field. The transition to quantum field theory is made by promoting the fields ϕ and π to Hermitian operators that satisfy certain equal-time commutation relations.

Suppose that, for example, $\phi = 0$ on the boundary ∂V. The condition $\phi = 0$ on the boundary is called the homogeneous Dirichlet condition. Inside V, ϕ can be expanded such that

$$\phi = \sum_{\mathbf{k}}\frac{1}{2\omega_{\mathbf{k}}V}\left(a_{\mathbf{k}}\exp(-i\,k\cdot x) + a^\dagger_{\mathbf{k}}\exp(i\,k\cdot x)\right), \tag{2.8}$$

where $\omega_{\mathbf{k}} = |\mathbf{k}|$ are the eigenenergies of the classical field equation subject to the homogeneous Dirichlet boundary condition. It follows from the commutation relations satisfied by ϕ and π that the creation and annihilation operators, $a^\dagger_{\mathbf{k}}$ and $a_{\mathbf{k}}$ respectively, satisfy

$$[a_{\mathbf{k}}, a^\dagger_{\mathbf{k}'}] = 2\omega_{\mathbf{k}} V \delta_{\mathbf{k}\mathbf{k}'}, \tag{2.9}$$

where δ is the Kronecker delta, and all other commutators vanish. In terms of the creation and annihilation operators, the Hamiltonian, now an operator, becomes

$$H = \frac{1}{2}\sum_{\mathbf{k}} \frac{1}{2\omega_{\mathbf{k}} V} \omega_{\mathbf{k}} \left(2a^\dagger_{\mathbf{k}} a_{\mathbf{k}} + [a_{\mathbf{k}}, a^\dagger_{\mathbf{k}}]\right). \tag{2.10}$$

The vacuum state is defined by $a_{\mathbf{k}}|0\rangle_{\partial V} = 0$ and normalized such that $\langle 0|0\rangle_{\partial V} = 1$. It follows that the expectation value of the Hamiltonian operator is

$$\langle 0|H|0\rangle_{\partial V} = \frac{1}{2}\sum_{\mathbf{k}} \omega_{\mathbf{k}}. \tag{2.11}$$

Clearly, the energy of the disturbed vacuum is divergent. Similar analysis shows that the energy of an equal volume of the undisturbed vacuum is also divergent. In order for the change in the zero-point energy to be well-defined, regularization and renormalization are required. These concepts are now discussed within the context of an example.

Example 1A (Two Dirichlet points; direct-summation method). Consider a massless real scalar field in one spatial dimension that satisfies the homogeneous Dirichlet condition at two points separated by a distance a. The eigenenergies of the disturbed vacuum are given by $\omega_n = \pi n/a$, where $n = 1, 2, \ldots$. The zero-point energy of the disturbed vacuum is

$$\langle 0|H|0\rangle_{\partial V} = \frac{\pi}{2a}\sum_{n=1}^{\infty} n. \tag{2.12}$$

This divergent sum can be regulated by inserting a regulating exponential factor,

$$\langle 0|H|0\rangle_{\partial V} = \frac{\pi}{2a}\sum_{n=1}^{\infty} n\exp(-\epsilon n). \tag{2.13}$$

The regulated expression (2.13) formally agrees with the original expression (2.12) when the regulating parameter ϵ is zero. However, if $\epsilon > 0$, then

$$\langle 0|H|0\rangle_{\partial V} = \frac{\pi}{8a}\,\mathrm{csch}^2\left(\frac{\epsilon}{2}\right). \tag{2.14}$$

Treating ϵ as a complex variable, and making a Laurent expansion about $\epsilon = 0$,

$$\langle 0|H|0\rangle_{\partial V} = \frac{\pi}{2a}\,\frac{1}{\epsilon^2} - \frac{\pi}{24a} + O(\epsilon^2)\,. \tag{2.15}$$

The zero-point energy of an equal volume of undisturbed vacuum is given by

$$\langle 0|H|0\rangle_0 = \frac{\pi}{2a}\int_0^\infty dx\, x\,. \tag{2.16}$$

Inserting the same regulating exponential factor,

$$\langle 0|H|0\rangle_0 = \frac{\pi}{2a}\int_0^\infty dx\, x \exp(-\epsilon x)\,. \tag{2.17}$$

If $\mathrm{Re}(\epsilon) > 0$, then

$$\langle 0|H|0\rangle_0 = \frac{\pi}{2a}\,\frac{1}{\epsilon^2}\,. \tag{2.18}$$

The renormalized zero-point energy is given by the limit as the regulating parameter tends to zero of the difference of the two regulated expressions (2.15) and (2.18). The result is

$$E = -\frac{\pi}{24a}\,. \tag{2.19}$$

In the simple one-dimensional example above, the indeterminate expression for the change in the zero-point energy was made well-defined by first regulating the expressions for the energy of the disturbed and undisturbed vacuum, and then renormalizing the difference. The generalization of this procedure is taken to be the definition of zero-point energy used in this thesis.

Definition. *The change in the zero-point energy is the regulated and renormalized difference of the energy of the disturbed vacuum with respect to the energy of an equal volume of the undisturbed vacuum.*

Since the difference is always taken with respect to an equal volume of the undisturbed vacuum, often 'the change in' is taken as understood and the renormalized difference is referred to as simply the zero-point energy.

This section is concluded with a brief discussion on two methods that are similar to the direct-summation method: the Euler-Maclaurin method and the Abel-Plana method. Both of these methods replace the difference between the summation and its corresponding integral with a new expression that can then be evaluated.

Example 1B (Two Dirichlet points; Euler-Maclaurin method). For the one-dimensional example, the renormalized zero-point energy can be given by

$$E = \lim_{\epsilon \to 0} \left(\sum_{n=1}^{\infty} f(n) - \int_0^{\infty} dx\, f(x) \right), \tag{2.20}$$

where $f(x) = \pi x \exp(-\epsilon x)/(2a)$. The difference between the summation and integration can be evaluated using the Euler-Maclaurin formula [33],

$$\sum_{n=1}^{\infty} f(n) - \int_0^{\infty} dx\, f(x) = \frac{f(\infty) + f(0)}{2} + \sum_{k=1}^{\infty} \frac{B_{2k}}{(2k)!} \left(f^{(2k-1)}(\infty) - f^{(2k-1)}(0) \right), \tag{2.21}$$

where B_{2k} are the Bernoulli numbers. The only term that survives in the limit as ϵ tends to zero is $f^{(1)}(0) = \pi/(2a)$. Therefore,

$$E = -\frac{\pi}{4a} B_2 . \tag{2.22}$$

The result (2.19) follows immediately, since $B_2 = 1/6$.

Example 1C (Two Dirichlet points; Abel-Plana method). The result can also be obtained using the Abel-Plana method. Recall that, formally,

$$E = \sum_{n=1}^{\infty} f(n) - \int_0^{\infty} dx\, f(x) , \tag{2.23}$$

where $f(x) = \pi x/(2a)$. The Abel-Plana method replaces the difference between the sum and integral with another integral,

$$E = \frac{f(0)}{2} + i\int_0^\infty dz \frac{f(iz) - f(-iz)}{\exp(2\pi z) - 1}. \tag{2.24}$$

There is no need for the regulating exponential factor; the renormalization is hidden in the derivation of the Abel-Plana method, which uses the argument theorem. With $f(x) = \pi x/(2a)$,

$$E = -\frac{\pi}{a}\int_0^\infty dz \frac{z}{\exp(2\pi z) - 1}. \tag{2.25}$$

Scaling z by a factor of $1/(2\pi)$,

$$E = -\frac{1}{4\pi a}\int_0^\infty dz \frac{z}{\exp(z) - 1}. \tag{2.26}$$

This integral can be evaluated in terms of the Gamma function and Riemann zeta function,

$$E = -\frac{1}{4\pi a}\zeta_R(2)\Gamma(2). \tag{2.27}$$

Again, the result (2.19) follows immediately, since $\zeta_R(2) = \pi^2/6$ and $\Gamma(2) = 1$.

2.3 Green-function method

Recall that the Hamiltonian is given by

$$H = \frac{1}{2}\int_V d^3x\left(\partial_0\phi\partial^0\phi - \phi\partial_0\partial^0\phi\right) + \frac{1}{2}\int_{\partial V} dS\,\phi\,\mathbf{n}\cdot\nabla\phi. \tag{2.28}$$

Assuming that the field ϕ is suitably well-behaved at spatial infinity, the total Hamiltonian, the Hamiltonian for all space, reduces to

$$H = \frac{1}{2}\int d^3x\left(\partial_0\phi\partial^0\phi - \phi\partial_0\partial^0\phi\right). \tag{2.29}$$

Let x and x' be non-coincident events. The total Hamiltonian can be formally recovered by

$$H = \frac{1}{2}\int d^3x \lim_{x'\to x}\left(\partial_0\partial'^0 - \partial'_0\partial'^0\right)\phi(x)\phi(x'). \tag{2.30}$$

After making the transition to quantum field theory, the expectation value of the total Hamiltonian operator is

$$\langle 0|H|0\rangle = \frac{1}{2}\int d^3x \lim_{x'\to x}\left(\partial_0\partial'^0 - \partial'_0\partial'^0\right)\langle 0|\phi(x)\phi(x')|0\rangle\,. \tag{2.31}$$

The integrand is related to the Feynman Green function G [34]. In particular, for $t > t'$,

$$\langle 0|\phi(x)\phi(x')|0\rangle = \frac{1}{i}\,\mathrm{G}(x,x'). \tag{2.32}$$

The Feynman Green function satisfies

$$\partial_\mu\partial^\mu\,\mathrm{G}(x,x') = \delta^4(x-x')\,. \tag{2.33}$$

In practice, the reduced Green function g is often used. The reduced Green function is related to G by

$$\mathrm{G}(x,x') = \int \frac{d\omega}{2\pi}\exp(-i\omega\tau)\,\mathrm{g}(\mathbf{x},\mathbf{x}')\,, \tag{2.34}$$

where $\tau = t - t'$ and the dependence of g on ω has been suppressed. Let $\mathrm{g}_{\partial V}$ denote the reduced Green function for the disturbed vacuum and g_0 denote that for the undisturbed vacuum. The change in the zero-point energy is given by

$$E = \lim_{\tau\to 0}\frac{1}{2\pi i}\int d\omega\,\exp(-i\omega\tau)\int d^3x\,\omega^2\,\mathrm{g}(\mathbf{x},\mathbf{x})\,, \tag{2.35}$$

where $\mathrm{g}(\mathbf{x},\mathbf{x}) = \mathrm{g}_{\partial V}(\mathbf{x},\mathbf{x}) - \mathrm{g}_0(\mathbf{x},\mathbf{x})$.

It is easy to show that the Green-function method is equivalent to regulating the sum of the classical eigenenergies with an oscillating exponential. Suppose that the vacuum is disturbed by the presence of some boundary ∂V. Let $\omega_{\mathbf{k}}$ and $\phi_{\mathbf{k}}$ denote the eigenenergies and eigenfunctions, respectively, of the scalar Helmholtz differential equation subject to the boundary condition. Assuming that the eigenfunctions are normalized such that

$$\int d^3x\,\phi_{\mathbf{k}}(\mathbf{x})\phi^*_{\mathbf{k}'}(\mathbf{x}) = \delta_{\mathbf{k}\mathbf{k}'} \tag{2.36}$$

and complete in the sense that

$$\sum_{\mathbf{k}}\phi_{\mathbf{k}}(\mathbf{x})\phi^*_{\mathbf{k}}(\mathbf{x}') = \delta^3(\mathbf{x}-\mathbf{x}')\,, \tag{2.37}$$

the reduced Green function can be formally given by [35]

$$\mathrm{g}_{\partial V}(\mathbf{x},\mathbf{x}') = \sum_{\mathbf{k}} \frac{\phi_{\mathbf{k}}(\mathbf{x})\phi_{\mathbf{k}}^*(\mathbf{x}')}{\omega_{\mathbf{k}}^2 - \omega^2}\,. \tag{2.38}$$

Using the normalization (2.36), the spatial integral of the reduced Green function becomes

$$\int d^3x\,\omega^2\,\mathrm{g}_{\partial V}(\mathbf{x},\mathbf{x}) = \sum_{\mathbf{k}} \frac{\omega^2}{\omega_{\mathbf{k}}^2 - \omega^2}\,. \tag{2.39}$$

Introducing the dimensionless variable $z = \omega a$, where a is a positive length scale,

$$\langle 0|H|0\rangle_{\partial V} = \lim_{\delta\to 0}\frac{1}{a}\sum_{\mathbf{k}}\frac{1}{2\pi i}\int_{C_1} dz\,\frac{z^2\exp(-iz\delta)}{z_{\mathbf{k}}^2 - z^2}\,, \tag{2.40}$$

where $\delta = \tau/a$. To avoid the poles of the integrand on the real axis, the integration path is deformed. For the Feynman Green function, the integration path is deformed to lie just below the negative real axis and just above the positive real axis. Let C_1 denote this contour. Figure 2.1 shows the contour C_1 and another contour C_2. The contour C_2 is a semicircular arc in the lower half plane. Since $\tau > 0$, the integral along C_2 vanishes in the limit as the radius of the arc tends to infinity. Therefore, the energy of the disturbed vacuum can be given by the integral around C: the join of C_1 and C_2. The integrand is meromorphic throughout the complex plane with simple poles at $z = -z_{\mathbf{k}}$ and $z = z_{\mathbf{k}}$. The contour C encloses only the latter. Using Cauchy's theorem,

$$\frac{1}{2\pi i}\int_C dz\,\frac{z^2\exp(-iz\delta)}{z_{\mathbf{k}}^2 - z^2} = \frac{1}{2}z_{\mathbf{k}}\exp(-iz_{\mathbf{k}}\delta)\,. \tag{2.41}$$

Therefore,

$$\langle 0|H|0\rangle_{\partial V} = \lim_{\delta\to 0}\frac{1}{2a}\sum_{\mathbf{k}} z_{\mathbf{k}}\exp(-iz_{\mathbf{k}}\delta)\,. \tag{2.42}$$

Example 1D (Two Dirichlet points; Green-function method). Consider the simple one-dimensional example again. The reduced Green function for the disturbed vacuum is [23]

$$\mathrm{g}_{\partial V}(x,x) = -\frac{\sin(|\omega|(x+a/2))\sin(|\omega|(x-a/2))}{|\omega|\sin(|\omega|a)}\,. \tag{2.43}$$

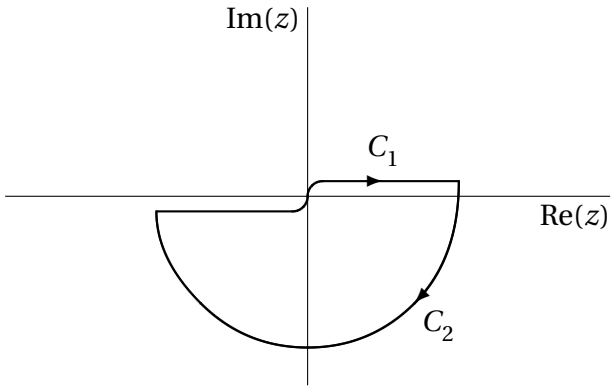

Figure 2.1: The contours C_1 and C_2.

The spatial integral is

$$\int_{-a/2}^{a/2} dx\,\omega^2\,\mathrm{g}_{\partial V}(x,x) = \frac{1}{2} - \frac{|\omega|a}{2}\cot(|\omega|a)\,. \tag{2.44}$$

The first term is independent of a and therefore does not depend on the boundary. Consequently, this term may be omitted. Introducing the dimensionless variable $z = \omega a$,

$$\int_{-a/2}^{a/2} dx\,\omega^2\,\mathrm{g}_{\partial V}(x,x) = -\frac{|z|}{2}\cot(|z|)\,. \tag{2.45}$$

The corresponding result for the undisturbed vacuum is

$$\int_{-a/2}^{a/2} dx\,\omega^2\,\mathrm{g}_{0}(x,x) = \frac{i|z|}{2}\,. \tag{2.46}$$

The zero-point energy is

$$E = \lim_{\tau\to 0}\frac{1}{a}\frac{1}{2\pi i}\int dz\,\exp(-iz\tau/a)\left(-\frac{|z|}{2}\cot(|z|) - \frac{i|z|}{2}\right). \tag{2.47}$$

In this case, the regulating parameter may be set equal to zero; that is,

$$E = \frac{1}{a}\frac{1}{2\pi i}\int dz\left(-\frac{|z|}{2}\cot(|z|) - \frac{i|z|}{2}\right). \tag{2.48}$$

Now the integrand is even with respect to z. Consequently, the integral can be given by twice the integral over positive z, and the absolute values can be dropped. To avoid the poles of the integrand, z is treated as a complex variable and the integration path

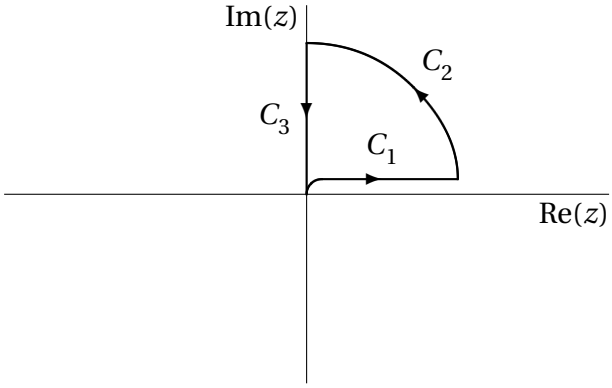

Figure 2.2: The contours C_1, C_2 and C_3.

is deformed to lie just above the positive real axis. Let C_1 denote this contour. Suppose that this contour is closed in the first quadrant, as shown in figure 2.2. The contour C_2 is a quarter-circular arc in the first quadrant. The contour C_3 is along the positive imaginary axis. Let C denote the join of the three contours C_1, C_2 and C_3. The integrand has no poles within or on C. Consequently, using Cauchy's theorem, the integral around C is zero. It is straightforward to show that in the limit as the radius of the arc tends to infinity the integral along C_2 is zero. It follows then, that the zero-point energy can be given by an integral along the positive imaginary axis,

$$E = -\frac{1}{2\pi a}\int_0^\infty dy\,\big(y\coth(y) - y\big). \tag{2.49}$$

This procedure is sometimes called a Euclidean or Wick rotation. Expressing the hyperbolic cotangent in terms of the exponential function,

$$E = -\frac{1}{4\pi a}\int_0^\infty dy\,\frac{y}{\exp(y)-1}, \tag{2.50}$$

which agrees with equation (2.26), from which the result (2.19) follows.

Related to the Green-function method is the method of images [36]. In this method the reduced Green function for the disturbed vacuum is constructed from a series of reduced Green functions for the undisturbed vacuum.

Example 1E (Two Dirichlet points; method of images). Consider the simple one-dimensional example again. Let x and x' be two noncoincident points inside the boundary. The reduced Green function between these two points is given by the reduced Green function for the undisturbed vacuum,

$$\mathrm{g}_0(x,x') = \frac{i\exp(i|\omega||x-x'|)}{2|\omega|}. \tag{2.51}$$

Now consider a path between the two points that includes a reflection at one of the boundary points. This path is equivalent to the path between one of the points and the image of the other. A path that includes a double reflection is equivalent to the path between one point and the image of the image of the other; and so on. For this example, only even reflections contribute to the zero-point energy [36]. The sum of all the even reflections is

$$\mathrm{g}_{\partial V}(x,x') = \sum_{n=-\infty}^{\infty} \mathrm{g}_0(x,x'-2an). \tag{2.52}$$

Since the summation is even with respect to n,

$$\mathrm{g}_{\partial V}(x,x') = \mathrm{g}_0(x,x') + 2\sum_{n=1}^{\infty} \mathrm{g}_0(x,x'-2an). \tag{2.53}$$

Removing the reduced Green function for the undisturbed vacuum, and letting the spatial points coincide,

$$\mathrm{g}(x,x) = \sum_{n=1}^{\infty} \frac{i\exp(2i|\omega|an)}{|\omega|}. \tag{2.54}$$

Following the Green-function method, the spatial integral is

$$\int_{-a/2}^{a/2} dx\,\omega^2\,\mathrm{g}(x,x) = i|\omega|a\sum_{n=1}^{\infty}\exp(2i|\omega|an) \tag{2.55}$$

This expression is even with respect to ω. Again, the frequency integral is replaced by twice the integral over positive frequency. This, in turn, is expressed in terms of an integral along the positive imaginary axis. The result is that the zero-point energy is

$$E = -\frac{1}{\pi a}\int_0^{\infty} dy \sum_{n=1}^{\infty} y\exp(-2yn). \tag{2.56}$$

Interchanging the order of summation and integration, and performing the straightforward integration,

$$E = -\frac{1}{4\pi a}\sum_{n=1}^{\infty}\frac{1}{n^2}. \tag{2.57}$$

Recognizing the summation as $\zeta_R(2) = \pi^2/6$, the result (2.19) is recovered.

The method of images is restricted to simple boundaries such as parallel planes. A similar method that can be used for more complicated boundaries is the multiple-reflection method. The multiple-reflection method is similar to the method of images in that the reduced Green function for the disturbed vacuum is expanded in terms of the reduced Green function of the undisturbed vacuum. The expansion is in the form of a series of iterated integrals over the boundary. Each term in the series corresponds to including another reflection. In principle, the multiple-reflection expansion is exact; however, that also means that, in general, it offers no computational advantage. The multiple-reflection method is useful because reasonable approximate results can be obtained by truncating the series [28]. The multiple-reflection method can also be used for boundaries that are not separable. For the one-dimensional example the multiple-reflection method is equivalent to the method of images.

Another reasonably accurate approximation can be made by including only optical paths; that is, ignoring diffraction [37]. Again, for the one-dimensional example the optical-path approximation is equivalent to the method of images.

2.4 Zeta-function method

Recall that the energy of the disturbed vacuum is given by

$$\langle 0|H|0\rangle_{\partial V} = \frac{1}{2}\sum_{\mathbf{k}}\omega_{\mathbf{k}}, \tag{2.58}$$

where ω_{k} are the eigenenergies of the classical field equation. Let

$$\zeta(s) = \mu^s\sum_{\mathbf{k}}\omega_{\mathbf{k}}^{-s}, \tag{2.59}$$

where s is a complex variable and μ is a positive mass scale. Then, expression (2.58) can be formally recovered by

$$\langle 0|H|0\rangle_{\partial V} = \frac{1}{2}\mu\zeta(-1)\,. \tag{2.60}$$

Typically, the zeta function (2.59) only converges for sufficiently large $\mathrm{Re}(s)$. Continuation is used to get to a neighbourhood of $s=-1$. Any divergence is removed using the principal-part prescription [38]. Practically, performing the principal-part prescription picks out the constant term in the Laurent expansion of the zeta function about $s=-1$. In terms of the principal-part prescription, the zero-point energy is

$$E = \frac{1}{2}\operatorname*{pp}_{s=-1}\mu\zeta(s)\,. \tag{2.61}$$

Example 1F (Two Dirichlet points; zeta-function method). The zeta function for the one-dimensional example can be written in terms of the Riemann zeta function,

$$\zeta(s) = \left(\frac{\mu a}{\pi}\right)^s \zeta_R(s)\,. \tag{2.62}$$

The Riemann zeta function can be continued meromorphically to the entire complex plane. In this case, the principal-part prescription is not needed; the zero-point is

$$E = \frac{\pi}{2a}\zeta_R(-1)\,. \tag{2.63}$$

The result (2.19) follows from the fact that $\zeta_R(-1) = -1/12$.

Related to the zeta function is the Poisson kernel [39]. The Poisson kernel T can be defined by

$$\mathrm{T}(t) = \sum_{\mathbf{k}} \exp(-t\omega_{\mathbf{k}}/\mu)\,, \tag{2.64}$$

where t is a dimensionless variable that should not be confused with time. Again, μ is a positive mass scale. The Poisson kernel is sometimes called the cylindrical kernel. In

terms of the Poisson kernel, the zero-point energy is

$$E = -\frac{1}{2}\operatorname*{pp}_{t=0}\left(\mu \mathrm{T}'(t)\right), \tag{2.65}$$

where the prime denotes differentiation with respect to t.

Example 1G (Two Dirichlet points; Poisson-kernel method). For the one-dimensional example,

$$\mathrm{T}(t) = \sum_{n=1}^{\infty} \exp\left(-\frac{\pi t n}{\mu a}\right). \tag{2.66}$$

If $\mathrm{Re}(t) > 0$, then

$$\mathrm{T}(t) = \frac{1}{\exp\left(\frac{\pi t}{\mu a}\right) - 1}. \tag{2.67}$$

This expression can be easily continued to other t. The derivative is

$$\mathrm{T}'(t) = -\frac{\pi}{4a}\,\mathrm{csch}^2\left(\frac{\pi t}{2\mu a}\right). \tag{2.68}$$

Treating t as a complex variable, and making a Laurent expansion about $t = 0$,

$$\mathrm{T}'(t) = -\frac{\mu a}{\pi}\frac{1}{t^2} + \frac{\pi}{12\mu a} + O(t^2). \tag{2.69}$$

The principal-part prescription picks out the term independent of t, and the zero-point energy (2.19) is recovered.

The Poisson kernel and the zeta function are related through the expression

$$\zeta(s)\Gamma(s) = \int_0^\infty dt\, t^{s-1}\,\mathrm{T}(t). \tag{2.70}$$

The Poisson kernel has a well-known expansion for small t [39]. The coefficients of the expansion depend on the type of field, the boundary, and the boundary condition. Using the relation (2.70), the divergence of the zeta function can be studied in terms of the coefficients of the Poisson-kernel expansion. In fact, it is this relationship with the zeta function that is the primary use of the Poisson kernel. It is only because the

one-dimensional example is so simple that it could be used to calculate the zero-point energy.

Some authors prefer to define the zeta function by

$$\zeta(s) = (\mu)^{2s} \sum_{\mathbf{k}} \omega_{\mathbf{k}}^{-2s}. \tag{2.71}$$

Rather than the Poisson kernel, this zeta function is related to the heat kernel K through the expression

$$\zeta(s)\Gamma(s) = \int_0^\infty dt\, t^{s-1}\, \mathrm{K}(t). \tag{2.72}$$

The heat kernel can also be expanded for small t, offering another way that the divergence of the zeta function can be studied.

This section is concluded with a brief discussion of the dimensional-regularization method. As the name suggests, the dimensional-regularization method uses the number of dimensions as the regulating parameter. It is included in this section because, like the zeta-function method, it uses continuation. The zero-point energy is evaluated for dimensions such that the generalized expression is well-defined. The result is then continued to the desired number of dimensions, such as the physical three spatial dimensions.

Example 1H (Two Dirichlet points; dimensional-regularization method). Recall that for the simple one-dimensional example, the eigenenergies are given by $\omega_n = \pi n/a$. Generalizing to parallel hyperplanes with D transverse dimensions, the eigenenergies are given by

$$\omega_{\mathbf{k}} = \sqrt{\mathbf{k}^2 + (\pi n/a)^2}. \tag{2.73}$$

where $\mathbf{k}^2 = k_1^2 + k_2^2 + \cdots + k_D^2$. Assuming that the hyperplanes are large compared with the separation between them, the summations over $k_1, k_2, \ldots, k_D$ can be replaced with integrals; that is,

$$E = \frac{L^D}{2\pi^D} \sum_{n=1}^{\infty} \int d^D k\, \sqrt{\mathbf{k}^2 + (\pi n/a)^2}. \tag{2.74}$$

Let $\mathscr{E}$ denote the energy per unit transverse hyperarea, $\mathscr{E} = E/L^D$. Scaling $\mathbf{k}$ by a factor of π/a,

$$\mathscr{E} = \frac{\pi}{2a^{D+1}} \sum_{n=1}^{\infty} \int d^D k \sqrt{\mathbf{k}^2 + n^2}\,. \tag{2.75}$$

Using [19]

$$\int d^D k\, f(\mathbf{k}) = \frac{2\pi^{\frac{D}{2}}}{\Gamma\left(\frac{D}{2}\right)} \int dk\, k^{D-1} f(k)\,, \tag{2.76}$$

the zero-point energy becomes

$$\mathscr{E} = -\frac{\pi^{\frac{D+1}{2}} \Gamma\left(-\frac{D+1}{2}\right)}{2^{D+2} a^{D+1}} \sum_{n=1}^{\infty} n^{D+1}\,. \tag{2.77}$$

Recognizing the summation as the Riemann zeta function,

$$\mathscr{E} = -\frac{\pi^{\frac{D+1}{2}} \Gamma\left(-\frac{D+1}{2}\right) \zeta_R(-D-1)}{2^{D+2} a^{D+1}}\,. \tag{2.78}$$

With $D = 0$ the result (2.19) is recovered.

2.5 Further examples

Example 2 (spherical boundary; Green-function method). In this example, the Green-function method is used to calculate the zero-point energy of a massless real scalar field that satisfies the homogeneous Dirichlet condition on the boundary of a sphere of radius R. Without any loss of generality, the boundary can be given by $(x, y, z) \in \mathbb{R}^3$ such that

$$x^2 + y^2 + z^2 = R^2\,. \tag{2.79}$$

It is convenient to work in spherical coordinates (r, θ, φ), which are related to Cartesian coordinates by

$$x = r \sin(\theta) \cos(\varphi)\,, \tag{2.80}$$

$$y = r \sin(\theta) \sin(\varphi)\,, \tag{2.81}$$

$$z = r \cos(\theta)\,. \tag{2.82}$$

The domains are $0 \le r < \infty$, $0 < \theta < \pi$ and $0 < \varphi < 2\pi$. In spherical coordinates, the boundary (2.79) is given by $r = R$. The boundary separates space into two regions. Let region I denote inside the boundary and region II denote outside the boundary.

The reduced Green function for this example in the interior of the boundary is [35]

$$\mathrm{g}^{\mathrm{I,D}}(\mathbf{x},\mathbf{x}') = -i|\omega| \sum_{l=0}^{\infty} \sum_{m=-l}^{l} \mathrm{Y}_l^m(\theta,\varphi)\, \mathrm{Y}_l^{m*}(\theta',\varphi') \frac{\mathrm{h}_l(|\omega|R)}{\mathrm{j}_l(|\omega|R)} \mathrm{j}_l(|\omega|r)\, \mathrm{j}_l(|\omega|r')\,, \tag{2.83}$$

where Y_l^m are the spherical harmonics, j_l are the spherical Bessel functions of the first kind, and $\mathrm{h}_l = \mathrm{h}_l^{(1)}$ are the spherical Hankel functions of the first kind. The superscripts on the reduced Green function refer to region I and the Dirichlet condition, respectively. The reduced Green function for the exterior of the boundary is identical except that the spherical Bessel and spherical Hankel functions are interchanged.

For simplicity, the regulating parameter is set equal to zero; any divergence is removed using continuation. With $\delta = 0$,

$$E^{\mathrm{D}} = \frac{1}{2\pi i} \int d\omega \int d^3x\, \omega^2\, \mathrm{g}(\mathbf{x},\mathbf{x})\,. \tag{2.84}$$

The spatial integral, which is the integrand of the frequency integral, is an even function of the frequency. Consequently, the frequency integral can be given by twice the integral over positive frequencies, and the absolute values in the reduced Green function can be dropped. Splitting the spatial integration into region I and region II, and scaling r by a factor of $1/\omega$,

$$\begin{aligned} \int d^3x\, \omega^2\, \mathrm{g}(\mathbf{x},\mathbf{x}) = -i \sum_{l=0}^{\infty} \sum_{m=-l}^{l} \int_0^{2\pi} d\varphi \int_0^{\pi} d\theta\, \sin(\theta)\, \mathrm{Y}_l^m(\theta,\varphi)\, \mathrm{Y}_l^{m*}(\theta,\varphi) \\ \times \left(\frac{\mathrm{h}_l(\omega R)}{\mathrm{j}_l(\omega R)} \int_0^{\omega R} dr\, r^2 \big(\mathrm{j}_l(r)\big)^2 + \frac{\mathrm{j}_l(\omega R)}{\mathrm{h}_l(\omega R)} \int_{\omega R}^{\infty} dr\, r^2 \big(\mathrm{h}_l(r)\big)^2 \right). \end{aligned} \tag{2.85}$$

The angular integration can be performed using the normalization of the spherical harmonics [40]. The radial integration can be performed using the recurrence relations of the spherical Bessel and spherical Hankel functions. Introducing the dimensionless variable $z = \omega R$, and simplifying,

$$\int d^3x\, \omega^2\, \mathrm{g}(\mathbf{x},\mathbf{x}) = -\sum_{l=0}^{\infty} \frac{2l+1}{2} \left(\frac{z\mathrm{j}_l'(z)}{\mathrm{j}_l(z)} + \frac{z\mathrm{h}_l'(z)}{\mathrm{h}_l(z)} + 1 \right), \tag{2.86}$$

where the prime denotes differentiation with respect to z.

The last term in the brackets is independent of z and therefore independent of R. Since this term does not depend on the boundary, it can be omitted from the expression for the zero-point energy. However, not only is this constant term kept, but also doubled for later convenience.

The zero-point energy is

$$E^{\mathrm{D}}(R) = -\frac{2}{R}\sum_{l=0}^{\infty}\frac{2l+1}{2}\frac{1}{2\pi i}\int dz\left(\frac{z\,\mathrm{j}_l'(z)}{\mathrm{j}_l(z)}+\frac{z\,\mathrm{h}_l'(z)}{\mathrm{h}_l(z)}+2\right). \tag{2.87}$$

The two in the prefactor is because the integration is over positive frequency only. Following the same argument as in example 1D, this integral can be expressed in terms of an integral along the positive imaginary axis. To avoid the poles of the integrand, z is treated as a complex variable and the integration path is deformed to lie just above the positive real axis. The contour is then closed in the first quadrant; see figure 2.2. Let C denote the join of the three contours C_1, C_2 and C_3. Since the integrand has no poles within or on C [40], the integral around C is zero. It remains to show that the integral along C_2 is also zero.

The contour C_2 is a quarter-circular arc of radius ρ, where $\rho\to\infty$. For large $|z|$ with $\mathrm{Im}(z)>0$ [40],

$$\mathrm{j}_l(z) \sim \frac{i^{l+1}\exp(-iz)}{2z}\left(1-\frac{il(l+1)}{2}\frac{1}{z}+O(z^{-2})\right), \tag{2.88}$$

$$\mathrm{h}_l(z) \sim \frac{(-i)^{l+1}\exp(iz)}{z}\left(1+\frac{il(l+1)}{2}\frac{1}{z}+O(z^{-2})\right). \tag{2.89}$$

These expansions are known as Hankel expansions. Using the Hankel expansions, it follows that the behavior of the integrand along the contour C_2 is

$$\frac{z\,\mathrm{j}_l'(z)}{\mathrm{j}_l(z)}+\frac{z\,\mathrm{h}_l'(z)}{\mathrm{h}_l(z)}+2 \sim O(z^{-2}). \tag{2.90}$$

Approximating the integral,

$$\left|\frac{1}{2\pi i}\int_{C_2} dz\left(\frac{z\,\mathrm{j}_l'(z)}{\mathrm{j}_l(z)}+\frac{z\,\mathrm{h}_l'(z)}{\mathrm{h}_l(z)}+2\right)\right| \sim O(\rho^{-1}), \tag{2.91}$$

which vanishes in the limit as $\rho \to \infty$. Since the integral along C_2 is zero, and the integral around C is zero, the zero-point energy can be written in terms of an integral along the positive imaginary axis. With $z = i\nu y$, where $\nu = l + 1/2$,

$$E^{\mathrm{D}}(R) = -\frac{1}{\pi R}\sum_{l=0}^{\infty}\int_0^{\infty} dy\, \nu^2\left(\frac{y\,\mathrm{i}_l'(\nu y)}{\mathrm{i}_l(\nu y)} + \frac{y\,\mathrm{k}_l'(\nu y)}{\mathrm{k}_l(\nu y)} + 2\right), \tag{2.92}$$

where the prime denotes differentiation with respect to y.

For large l [40],

$$\mathrm{i}_l(\nu y) \sim \frac{t\exp(\nu\eta)}{2\nu(1-t^2)^{1/4}}\left(1 + \frac{3t-5t^3}{24}\frac{1}{\nu} + \frac{81t^2-462t^4+385t^6}{1152}\frac{1}{\nu^2} + O(\nu^{-3})\right), \tag{2.93}$$

$$\mathrm{k}_l(\nu y) \sim \frac{t\exp(-\nu\eta)}{\nu(1-t^2)^{1/4}}\left(1 - \frac{3t-5t^3}{24}\frac{1}{\nu} + \frac{81t^2-462t^4+385t^6}{1152}\frac{1}{\nu^2} + O(\nu^{-3})\right), \tag{2.94}$$

where

$$t = \frac{1}{\sqrt{1+y^2}}, \tag{2.95}$$

$$\eta = \frac{1}{t} + \frac{1}{2}\ln\left(\frac{1-t}{1+t}\right). \tag{2.96}$$

These expansions are known as Debye expansions. Using the Debye expansions, it follows that the behaviour of the integrand for large l is

$$\nu^2\left(\frac{y\,\mathrm{i}_l'(\nu y)}{\mathrm{i}_l(\nu y)} + \frac{y\,\mathrm{k}_l'(\nu y)}{\mathrm{k}_l(\nu y)} + 2\right) \sim \frac{1}{1+y^2}\nu^2 - \frac{4y^2-10y^4+y^6}{4(1+y^2)^4} + O(\nu^{-2}). \tag{2.97}$$

The first two terms are subtracted from the integrand and then added back as a separate integral as follows

$$\begin{aligned} E^{\mathrm{D}}(R) = -\frac{1}{\pi R}\sum_{l=0}^{\infty}\int_0^{\infty} dy \Bigg(&\nu^2\left(\frac{y\,\mathrm{i}_l'(\nu y)}{\mathrm{i}_l(\nu y)} + \frac{y\,\mathrm{k}_l'(\nu y)}{\mathrm{k}_l(\nu y)} + 2\right) \\ &- \left(\frac{1}{1+y^2}\nu^2 - \frac{4y^2-10y^4+y^6}{4(1+y^2)^4}\right)\Bigg) \\ &- \frac{1}{\pi R}\sum_{l=0}^{\infty}\int_0^{\infty} dy\left(\frac{1}{1+y^2}\nu^2 - \frac{4y^2-10y^4+y^6}{4(1+y^2)^4}\right). \end{aligned} \tag{2.98}$$

Since the Debye expansions are uniform with respect to y [40], the first integral is $O(\nu^{-2})$ for large l. Consequently the subsequent summation converges by the comparison test. The second integral is straightforward; the subsequent summations can

be expressed in terms of the Hurwitz zeta function ζ_H using

$$\sum_{l=0}^{\infty} \nu^{-s} = \zeta_H(s, 1/2)\,, \tag{2.99}$$

which is valid for $\mathrm{Re}(s) > 1$. Using continuation, $\zeta_H(-2, 1/2) = 0$ and $\zeta_H(0, 1/2) = 0$, which leaves

$$E^{\mathrm{D}}(R) = -\frac{1}{\pi R} \sum_{l=0}^{\infty} \int_0^{\infty} dy \left(\nu^2 \left(\frac{y\, \mathrm{i}_l'(\nu y)}{\mathrm{i}_l(\nu y)} + \frac{y\, \mathrm{k}_l'(\nu y)}{\mathrm{k}_l(\nu y)} + 2 \right) - \left(\frac{1}{1+y^2} \nu^2 - \frac{4y^2 - 10y^4 + y^6}{4(1+y^2)^4} \right) \right). \tag{2.100}$$

Evaluating this expression,

$$E^{\mathrm{D}}(R) = \frac{0.00281\ldots}{R}\,, \tag{2.101}$$

which agrees with the result obtained by Bender and Milton [20].

If the result in example 1H, with $D = 2$, is multiplied by two, to take into account the two polarization states of the electromagnetic field, then Casimir's result is recovered. The same is not true for this example; multiplying the result (2.101) by two does not recover Boyer's result. For both boundaries, the electromagnetic field can be separated into two modes: transverse electric and transverse magnetic. These modes are equivalent to massless real scalar fields that satisfy certain conditions on the boundary. In the parallel planes case, the transverse electric mode satisfies the homogeneous Dirichlet condition on the boundary; the transverse magnetic mode satisfies the homogeneous Neumann condition on the boundary. The eigenenergies are the same for both boundary conditions. Consequently, combining the two modes is equivalent to simply multiplying the result for the Dirichlet boundary condition by two. For a spherical boundary, the eigenenergies of the two modes are different, which explains why Boyer's result can not be recovered so simply.

Example 3 (cylindrical boundary; zeta-function method). In this example, the zeta-function method is used to calculate the zero-point energy of a massless real scalar

field that satisfies the homogeneous Dirichlet condition on the boundary of a cylinder of radius R. Without any loss of generality, the boundary of a cylinder of radius R and infinite longitudinal length can be given by $(x, y, z) \in \mathbb{R}^3$ such that

$$x^2 + y^2 = R^2 . \tag{2.102}$$

It is convenient to work in cylindrical coordinates (r, θ, z), which are related to Cartesian coordinates by

$$x = r\cos(\theta) , \tag{2.103}$$

$$y = r\sin(\theta) , \tag{2.104}$$

and z is unchanged. The domains are: $0 \leq r < \infty$, $0 \leq \theta < 2\pi$ and $-\infty < z < \infty$. In cylindrical coordinates the boundary (2.102) is given by $r = R$. Again, let region I denote inside the boundary and region II denote outside the boundary.

The field equation, the scalar Helmholtz differential equation, is separable in cylindrical coordinates [35]. The general expression for the field in the interior of the boundary is

$$\phi^{\mathrm{I}} = \int_{-\infty}^{\infty} \frac{dk}{2\pi} \exp(ikz) \sum_{m=-\infty}^{\infty} A_m(k) \mathrm{J}_m(\lambda r) \exp(im\theta) , \tag{2.105}$$

where $\lambda = \sqrt{\omega^2 - k^2}$, A_m are arbitrary functions of the longitudinal momentum k, and J_m are the Bessel functions of the first kind.

The field satisfies the homogeneous Dirichlet conditions when

$$\mathrm{J}_m(\lambda R) = 0 . \tag{2.106}$$

Let λ_{mn} denote the positive solutions to (2.106). For sufficiently large $\mathrm{Re}(s)$, the zeta function for this problem can be given by

$$\zeta^{\mathrm{I,D}}(s, R) = \mu^s \int_{-\infty}^{\infty} \frac{dk}{2\pi} \sum_{m=-\infty}^{\infty} \sum_{n=1}^{\infty} \omega_{mn}^{-s} , \tag{2.107}$$

where $\omega_{mn} = \sqrt{\lambda_{mn}^2 + k^2}$. The integration with respect to k is straightforward. Using the relation

$$\int_{-\infty}^{\infty} \frac{dk}{2\pi} \left(\lambda_{mn}^2 + k^2\right)^{-s/2} = \frac{1}{2\pi} \mathrm{B}\left(\frac{s-1}{2}, \frac{1}{2}\right) \lambda_{mn}^{1-s} , \tag{2.108}$$

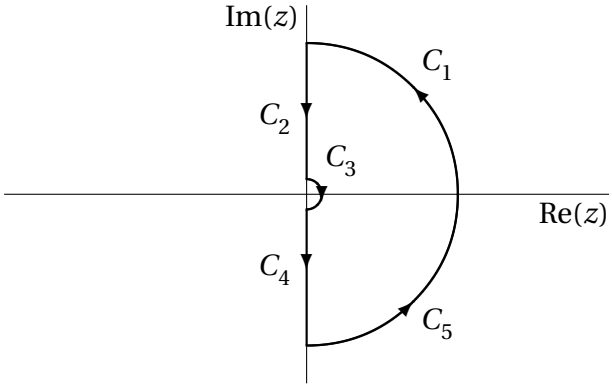

Figure 2.3: The five contours C_1 to C_5.

where B is the beta function, and introducing the dimensionless variable $z = \lambda R$, the zeta function becomes

$$\zeta^{\mathrm{I,D}}(s,R) = \frac{1}{2\pi}\,\mathrm{B}\left(\frac{s-1}{2},\frac{1}{2}\right)\frac{\mu^s}{R^{1-s}}\sum_{m=-\infty}^{\infty}\sum_{n=1}^{\infty} z_{mn}^{1-s}\,. \tag{2.109}$$

The zeros of the Bessel function are even with respect to m, so

$$\zeta^{\mathrm{I,D}}(s,R) = \frac{1}{2\pi}\,\mathrm{B}\left(\frac{s-1}{2},\frac{1}{2}\right)\frac{\mu^s}{R^{1-s}}\sum_{m=0}^{\infty}(2-\delta_{m0})\sum_{n=1}^{\infty} z_{mn}^{1-s}\,. \tag{2.110}$$

The summation with respect to n is absolutely convergent for $\mathrm{Re}(s) > 2$ [41]. Using the argument theorem [33],

$$\sum_{n=1}^{\infty} z_{mn}^{1-s} = \frac{1}{2\pi i}\int_C dz\, z^{1-s}\frac{\mathrm{J}'_m(z)}{\mathrm{J}_m(z)}\,, \tag{2.111}$$

where C is a closed contour, taken in the positive sense, that encloses all the positive zeros of the Bessel function and avoids the branch cut of the power function along the negative real axis. Figure 2.3 shows a suitable contour C made from the join of the five contours C_1 to C_5. The contours C_1 and C_5 are quarter-circular arcs of radius ρ, where $\rho \to \infty$. The contour C_3 is a semicircular arc of radius ϵ, where $0 < \epsilon < \min(z_{m1})$. The contours C_2 and C_4 are straight lines along the imaginary axis, joining the other contours. Each contour is now considered separately.

Using the Hankel expansion, the behaviour of the integrand along the contour C_1 is

$$z^{1-s}\frac{\mathrm{J}'_m(z)}{\mathrm{J}_m(z)} \sim -i\,z^{1-s} - \frac{1}{2}\,z^{-s} + O(z^{-1-s})\,. \tag{2.112}$$

Approximating the integral,

$$\left|\frac{1}{2\pi i}\int_{C_1} dz\, z^{1-s}\frac{\mathrm{J}'_m(z)}{\mathrm{J}_m(z)}\right| \sim O(\rho^{2-s}), \tag{2.113}$$

which, since $\mathrm{Re}(s) > 2$, vanishes in the limit as $\rho \to \infty$.

The Hankel expansion (2.112) is also used for the integral along the contour C_2. The first two terms are subtracted from the integrand and them added back as a separate integral; that is,

$$\begin{aligned}\frac{1}{2\pi i}\int_{C_2} dz\, z^{1-s}\frac{\mathrm{J}'_m(z)}{\mathrm{J}_m(z)} = \frac{1}{2\pi i}\int_{C_2} dz\left(z^{1-s}\frac{\mathrm{J}'_m(z)}{\mathrm{J}_m(z)} - \left(-iz^{1-s} - \frac{1}{2}z^{-s}\right)\right)\\ + \frac{1}{2\pi i}\int_{C_2} dz\left(-iz^{1-s} - \frac{1}{2}z^{-s}\right).\end{aligned} \tag{2.114}$$

On the imaginary axis $z = iy$. In the limit as $\rho \to \infty$,

$$\begin{aligned}\frac{1}{2\pi i}\int_{C_2} dz\, z^{1-s}\frac{\mathrm{J}'_m(z)}{\mathrm{J}_m(z)} = -\frac{i^{-s}}{2\pi}\int_\epsilon^\infty dy\, y^{1-s}\left(\frac{\mathrm{I}'_m(y)}{\mathrm{I}_m(y)} - \left(1 - \frac{1}{2y}\right)\right)\\ - \frac{i^{-s}}{2\pi}\left(\frac{\epsilon^{1-s}}{2(1-s)} - \frac{\epsilon^{2-s}}{2-s}\right),\end{aligned} \tag{2.115}$$

where I_m are the modified Bessel functions of the first kind.

The analysis for the integrals in the lower half plane is similar. Like the C_1 integral, the C_5 integral vanishes. The C_4 integral differs from the C_2 integral only by a phase. Combining all the contributions together,

$$\begin{aligned}\frac{1}{2\pi i}\int_C dz\, z^{1-s}\frac{\mathrm{J}'_m(z)}{\mathrm{J}_m(z)} = -\frac{1}{\pi}\cos\left(\frac{\pi s}{2}\right)\int_\epsilon^\infty dy\, y^{1-s}\left(\frac{\mathrm{I}'_m(y)}{\mathrm{I}_m(y)} - \left(1 - \frac{1}{2y}\right)\right)\\ - \frac{1}{\pi}\cos\left(\frac{\pi s}{2}\right)\left(\frac{\epsilon^{1-s}}{2(1-s)} - \frac{\epsilon^{2-s}}{2-s}\right)\\ + \frac{1}{2\pi i}\int_{C_3} dz\, z^{1-s}\frac{\mathrm{J}'_m(z)}{\mathrm{J}_m(z)}.\end{aligned} \tag{2.116}$$

The first term is holomorphic for $\mathrm{Re}(s) > 0$, the second term is meromorphic for all s, and the third term is holomorphic for all s. Expression (2.116) is therefore the continuation of the sum (2.111) to $\mathrm{Re}(s) > 0$.

Now suppose that s is restricted to the strip $0 < \mathrm{Re}(s) < 1$, and consider the limit as $\epsilon \to 0$. For $0 < \mathrm{Re}(s) < 1$, the second term vanishes in the limit as $\epsilon \to 0$. The third term

can be evaluated by

$$\lim_{\epsilon\to 0}\frac{1}{2\pi i}\int_{C_3} dz\, z^{1-s}\frac{\mathrm{J}'_m(z)}{\mathrm{J}_m(z)} = -\frac{1}{2}\operatorname*{res}_{z=0} z^{1-s}\frac{\mathrm{J}'_m(z)}{\mathrm{J}_m(z)}\,. \tag{2.117}$$

Using the Taylor expansion of the Bessel functions of the first kind [40],

$$z^{1-s}\frac{\mathrm{J}'_m(z)}{\mathrm{J}_m(z)} = m\,z^{-s} + O(z^{2-s})\,. \tag{2.118}$$

For $0 < \mathrm{Re}(s) < 1$, it follows that the residue is zero, and consequently the third term vanishes in the limit as $\epsilon \to 0$. The only remaining term is the first term. Therefore, for $0 < \mathrm{Re}(s) < 1$,

$$\sum_{n=1}^{\infty} z_{mn}^{1-s} = -\frac{1}{\pi}\cos\left(\frac{\pi s}{2}\right)\int_0^\infty dy\, y^{1-s}\left(\frac{\mathrm{I}'_m(y)}{\mathrm{I}_m(y)} - 1 + \frac{1}{2y}\right). \tag{2.119}$$

Return now to the zeta function. Separating out the $m = 0$ contribution,

$$\zeta^{\mathrm{I,D}}(s,R) = \frac{1}{2\pi}\,\mathrm{B}\left(-\frac{1-s}{2},\frac{1}{2}\right)\frac{\mu^s}{R^{1-s}}\left(\sum_{n=1}^{\infty} z_{0n}^{1-s} + 2\sum_{m=1}^{\infty}\sum_{n=1}^{\infty} z_{mn}^{1-s}\right). \tag{2.120}$$

Consider the $m = 0$ contribution. Using the meromorphic continuation (2.119),

$$\sum_{n=1}^{\infty} z_{0n}^{1-s} = -\frac{1}{\pi}\cos\left(\frac{\pi s}{2}\right)\int_0^\infty dy\, y^{1-s}\left(\frac{\mathrm{I}'_0(y)}{\mathrm{I}_0(y)} - 1 + \frac{1}{2y}\right). \tag{2.121}$$

The behaviour of the integrand for large y is

$$\frac{\mathrm{I}'_0(y)}{\mathrm{I}_0(y)} - 1 + \frac{1}{2y} \sim -\frac{1}{8}\frac{1}{1+y^2} - \frac{1}{8}\frac{1}{(1+y^2)^{3/2}} + O(y^{-4})\,. \tag{2.122}$$

Subtracting the first two terms from the integrand and then adding them back as a separate integral,

$$\begin{aligned}\sum_{n=1}^{\infty} z_{0n}^{1-s} = -\frac{1}{\pi}\cos\left(\frac{\pi s}{2}\right)\int_0^\infty dy\, y^{1-s}\left(\frac{\mathrm{I}'_0(y)}{\mathrm{I}_0(y)} - 1 + \frac{1}{2y} - \left(-\frac{1}{8}\frac{1}{1+y^2} - \frac{1}{8}\frac{1}{(1+y^2)^{3/2}}\right)\right)\\ -\frac{1}{\pi}\cos\left(\frac{\pi s}{2}\right)\int_0^\infty dy\, y^{1-s}\left(-\frac{1}{8}\frac{1}{1+y^2} - \frac{1}{8}\frac{1}{(1+y^2)^{3/2}}\right).\end{aligned} \tag{2.123}$$

The first integral is holomorphic for $-2 < \mathrm{Re}(s) < 1$. For $0 < \mathrm{Re}(s) < 1$, the second integral can be evaluated in terms of beta functions, which can be easily continued. The result is an expression for the $m = 0$ contribution that is valid in a neighbourhood of $s = -1$.

The analysis for the $m \neq 0$ contribution is similar. Since $m \neq 0$, y can be scaled by a factor of m,

$$2\sum_{m=1}^{\infty}\sum_{n=1}^{\infty} z_{mn}^{1-s} = -\frac{2}{\pi}\cos\left(\frac{\pi s}{2}\right)\sum_{m=1}^{\infty} m^{2-s}\int_0^{\infty} dy\, y^{1-s}\left(\frac{1}{m}\frac{\mathrm{I}_m'(my)}{\mathrm{I}_m(my)} - 1 + \frac{1}{2my}\right), \tag{2.124}$$

where the prime denotes differentiation with respect to y. Using the Debye expansion for the modified Bessel functions of the first kind [40],

$$\begin{aligned}\frac{1}{m}\frac{\mathrm{I}_m'(my)}{\mathrm{I}_m(my)} - 1 + \frac{1}{2my} \sim{}& \frac{\sqrt{1+y^2}-y}{y} + \frac{1}{2y(1+y^2)}\frac{1}{m} \\ &+ \frac{y(4-y^2)}{8(1+y^2)^{3/2}}\frac{1}{m^2} - \frac{y(4-10y^2+y^4)}{8(1+y^2)^4}\frac{1}{m^3} \\ &+ \frac{y(64-560y^2+456y^4-25y^6)}{128(1+y^2)^{11/2}}\frac{1}{m^4} + O(m^{-5}).\end{aligned} \tag{2.125}$$

In terms of integration, it is sufficient to subtract and add back only the first four terms of this expansion; however, to ensure that the subsequent summation with respect to m converges, it is necessary to subtract and add back at least the first five terms. Again, the result is an expression that is valid in a neighbourhood of $s = -1$.

Making a Laurent expansion of the zeta function about $s = -1$,

$$\zeta^{\mathrm{I,D}}(s,R) = -\frac{1}{315\pi\mu R^2}\frac{1}{s+1} + \frac{0.00066\ldots}{\mu R^2} - \frac{\ln(\mu R)}{315\pi\mu R^2} + O(s+1). \tag{2.126}$$

Using the principal-part prescription, the zero-point energy is

$$\mathscr{E}^{\mathrm{I,D}}(R) = \frac{0.00033\ldots}{R^2} - \frac{\ln(\mu R)}{630\pi R^2}. \tag{2.127}$$

The analysis for the field in the exterior of the boundary is similar. The general expression for the field in the exterior of the boundary is identical to that in the interior (2.105) except that the Bessel functions of the first kind are replaced with Hankel functions of the first kind. Repeating the analysis above, the result for the zero-point energy is

$$\mathscr{E}^{\mathrm{II,D}}(R) = \frac{0.00028\ldots}{R^2} + \frac{\ln(\mu R)}{630\pi R^2}. \tag{2.128}$$

The total zero-point energy is the sum of the interior and exterior contributions,

$$\mathscr{E}^{\mathrm{D}}(R) = \frac{0.00061\ldots}{R^2}, \tag{2.129}$$

which agrees with the result in [42].

The results for the zero-point energy in the interior and exterior of the boundary, (2.127) and (2.128) respectively, each contain a logarithmic term that depends on the mass scale μ. This remnant of the renormalization process should be regarded as a warning that in these cases the zero-point energy is in fact divergent. Only by considering both the internal and external contributions together is the total zero-point energy unambiguous.

The proper analysis for the field in the exterior of the boundary is considerably more complicated than what was presented here. Simply replacing the Bessel functions of the first kind with Hankel functions of the first kind leads to the eigenenergies being the zeros of the Hankel functions, which are complex. The more rigorous approach is to include another cylinder, concentric to the first and of larger radius. The eigenenergies in the annulus are then real. As the radius of the second cylinder tends to infinity, the result (2.128) is recovered. Since the results of the two approaches agree, only the simpler approach is discussed in this thesis.

Chapter 3

Elliptic-cylindrical boundary

3.1 Introduction

An elliptical cylinder is a cylinder whose cross-section is an ellipse. Without any loss of generality, the boundary of an elliptical cylinder can be given by $(x, y, z) \in \mathbb{R}^3$ such that

$$\frac{x^2}{a^2} + \frac{y^2}{b^2} = 1\,, \tag{3.1}$$

where the semimajor axis a is greater than the semiminor axis b, and both are nonzero.

It is convenient to work in elliptic-cylindrical coordinates. Using the notation in Abramowitz and Stegun [40], elliptic-cylindrical coordinates (u, v, z) are related to Cartesian coordinates by

$$x = f\cosh(u)\cos(v)\,, \tag{3.2}$$

$$y = f\sinh(u)\sin(v)\,, \tag{3.3}$$

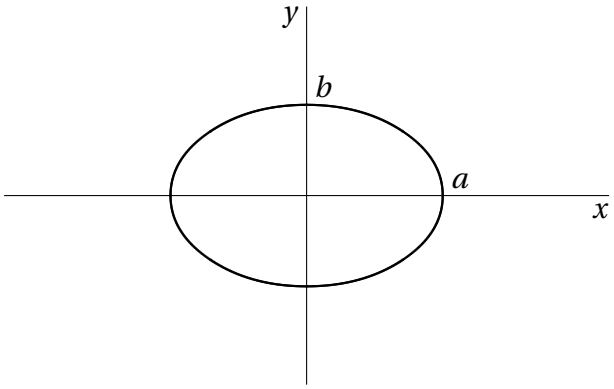

Figure 3.1: Cross-section of an elliptical cylinder.

where $f = \sqrt{a^2 - b^2}$, and z is unchanged. The domains are $0 \leq u < \infty$, $0 \leq v < 2\pi$ and $-\infty < z < \infty$. In elliptic-cylindrical coordinates, the boundary (3.1) is given implicitly by

$$\cosh(u) = \frac{1}{e}, \tag{3.4}$$

where $e = f/a$ is the eccentricity. To avoid confusion between eccentricity and the exponential function, the full form of the exponential function, exp, is used throughout this thesis.

Eccentricity can be thought of as a measure of how elliptical the elliptic-cylindrical boundary is. When the eccentricity is zero, the boundary reduces to that of a circular cylinder of radius a. In the opposite limit, as the eccentricity tends to one, the boundary becomes two parallel planes separated by a distance b. Because the limiting boundary is topologically different, it is likely that there is a discontinuity in the zero-point energy as the eccentricity tends to one. Consequently, only small eccentricity is considered.

The goal of this chapter is to calculate the change in the zero-point energy of the electromagnetic field subject to perfectly-conducting conditions on the boundary (3.1). First, a scalar field is considered.

3.2 Scalar field

3.2.1 Zeta-function method

Consider a massless real scalar field that satisfies the homogeneous Dirichlet condition on the boundary of the elliptical cylinder (3.1). Let region I denote the interior of the boundary and region II denote the exterior. The field equation, the scalar Helmholtz differential equation, is separable in elliptic-cylindrical coordinates [35]. The general

expression for the field in the interior of the boundary is [43]

$$\phi^{\mathrm{I}} = \int \frac{dk}{2\pi} \exp(ikz) \Bigg(\sum_{m=0}^{\infty} A_m(k)\, \mathrm{Mc}_m^{(1)}(u,q)\, \mathrm{ce}_m(v,q) + \sum_{m=1}^{\infty} B_m(k)\, \mathrm{Ms}_m^{(1)}(u,q)\, \mathrm{se}_m(v,q) \Bigg), \tag{3.5}$$

where $q = f^2\lambda^2/4$, $\lambda^2 = \omega^2 - k^2$; A_m and B_m are arbitrary functions of the longitudinal momentum k; $\mathrm{Mc}_m^{(1)}$ and $\mathrm{Ms}_m^{(1)}$ are the even and odd modified Mathieu functions of the first kind, respectively; and ce_m and se_m are the even and odd Mathieu functions, respectively. Mathieu functions are reviewed in appendix A.

The field satisfies the homogeneous Dirichlet condition on the boundary (3.4) when

$$\mathrm{Mc}_m^{(1)}(\operatorname{arccosh}(1/e), z^2e^2/4) = 0\,, \tag{3.6}$$

$$\mathrm{Ms}_m^{(1)}(\operatorname{arccosh}(1/e), z^2e^2/4) = 0\,. \tag{3.7}$$

Here, $z = \lambda a$ is a dimensional variable that should not be confused with the Cartesian coordinate. It follows that the zeta function for this problem, in the contour integral representation, is

$$\zeta^{\mathrm{I,D}}(s,a,e) = \frac{1}{2\pi}\mathrm{B}\left(\frac{s-1}{2},\frac{1}{2}\right)\frac{\mu^s}{a^{1-s}} \sum_{m=0}^{\infty} \frac{1}{2\pi i}\int_C dz\, z^{1-s} \Bigg(\frac{\mathrm{Mc}_m^{(1)\prime}(\operatorname{arccosh}(1/e), z^2e^2/4)}{\mathrm{Mc}_m^{(1)}(\operatorname{arccosh}(1/e), z^2e^2/4)} + \frac{\mathrm{Ms}_m^{(1)\prime}(\operatorname{arccosh}(1/e), z^2e^2/4)}{\mathrm{Ms}_m^{(1)}(\operatorname{arccosh}(1/e), z^2e^2/4)} \Bigg), \tag{3.8}$$

where the prime denotes differentiation with respect to z. For simplicity, let the contour C be the same contour used in example 3 in chapter 2. Using the results in appendix A, the formal expansion of the integrand is

$$\begin{aligned} &z^{1-s}\left(\frac{\mathrm{Mc}_m^{(1)\prime}(\operatorname{arccosh}(1/e), z^2e^2/4)}{\mathrm{Mc}_m^{(1)}(\operatorname{arccosh}(1/e), z^2e^2/4)} + \frac{\mathrm{Ms}_m^{(1)\prime}(\operatorname{arccosh}(1/e), z^2e^2/4)}{\mathrm{Ms}_m^{(1)}(\operatorname{arccosh}(1/e), z^2e^2/4)} \right) \\ &\qquad \sim (2-\delta_{m0})\left(z^{1-s}\frac{\mathrm{J}_m'(z)}{\mathrm{J}_m(z)} + \frac{1}{4}\left((1-s)z^{1-s}\frac{\mathrm{J}_m'(z)}{\mathrm{J}_m(z)} - \left(z^{2-s}\frac{\mathrm{J}_m'(z)}{\mathrm{J}_m(z)} \right)' \right) e^2 + O(e^4) \right). \end{aligned} \tag{3.9}$$

The leading term reproduces the integrand for a circular-cylindrical boundary of radius a (2.111). The first part of the next-to-leading term is proportional to the leading

term. The second part of the next-to-leading term is continuous throughout C, has an antiderivative, and consequently, since the contour is closed, does not contribute to the zeta function. Integrating termwise,

$$\zeta^{\mathrm{I,D}}(s,a,e) \sim \zeta^{\mathrm{I,D}}(s,a,0)\left(1+\frac{1-s}{4}\,e^2+O(e^4)\right). \tag{3.10}$$

The analysis for the field in the exterior of the boundary is similar. The general expression for the field in the exterior of the boundary is identical to that for the field in the interior of the boundary (3.5), except that the even and odd modified Mathieu functions of the first kind are replaced with those of the third kind. The subsequent analysis is also similar, except that Bessel functions of the first kind are replaced with Hankel functions of the first kind. The result for the zeta function is

$$\zeta^{\mathrm{II,D}}(s,a,e) \sim \zeta^{\mathrm{II,D}}(s,a,0)\left(1+\frac{1-s}{4}\,e^2+O(e^4)\right). \tag{3.11}$$

The total zeta function is given by the sum of the internal and external contributions. Since the eccentricity expansion is the same in both regions,

$$\zeta^{\mathrm{D}}(s,a,e) \sim \zeta^{\mathrm{D}}(s,a,0)\left(1+\frac{1-s}{4}\,e^2+O(e^4)\right). \tag{3.12}$$

The prefactor is the total zeta function for a massless scalar field that satisfies the homogeneous Dirichlet condition on the boundary of a circular cylinder of radius a, which was shown in example 3 in chapter 2 to be well-behaved at $s=-1$. Therefore, in this case, the principal-part prescription simplifies to straightforward substitution. The zero-point energy per unit longitudinal length of an elliptical cylinder is

$$\mathscr{E}^{\mathrm{D}}(a,e) \sim \mathscr{E}^{\mathrm{D}}(a,0)\left(1+\frac{1}{2}\,e^2+O(e^4)\right). \tag{3.13}$$

This result agrees with the work by Kvitsinsky [44], as shown in [45].

The result is now confirmed using a method that uses conformal mapping.

3.2.2 Conformal-map method

The elliptic-cylindrical boundary is inherently two-dimensional. If the longitudinal contribution is factored out, then the field equation reduces to

$$\left(\nabla^2 + \lambda_m^2\right)\phi_m = 0\,, \tag{3.14}$$

where the Laplacian is the two-dimensional Laplacian, and the homogeneous Dirichlet condition is imposed on the boundary of the ellipse (3.1).

Let us treat the Cartesian xy-plane as the complex $z = x + iy$ plane. The aim of this subsection is to map the problem in z-space onto one whose boundary is a circle of radius R. Such a map exists and is given by [46]

$$w(z) = R\sqrt{k}\,\mathrm{sn}\left(\frac{2\,\mathrm{K}(k^2)}{\pi}\arcsin\left(\frac{z}{\sqrt{a^2-b^2}}\right)\right), \tag{3.15}$$

where sn is the Jacobi elliptic function, K is the complete elliptic integral of the first kind and k, which should not be confused with momentum, depends on the semiaxes in terms of theta functions

$$k = \left(\frac{\vartheta_2(h)}{\vartheta_3(h)}\right)^2, \tag{3.16}$$

$$h = \left(\frac{a-b}{a+b}\right)^2. \tag{3.17}$$

Figure 3.2 shows how the conformal map maps z-space onto w-space.

Using the conformal map (3.15), the field equation in w-space is

$$\left(|w'|^2\nabla^2 + \lambda_m^2\right)\phi_m(w) = 0\,, \tag{3.18}$$

where the prime denotes differentiation with respect to z, and the Dirichlet condition is now imposed on the boundary of a circle of radius R. The problem in w-space is now considered for small eccentricity.

For small eccentricity,

$$k \sim e^2 + O(e^4)\,. \tag{3.19}$$

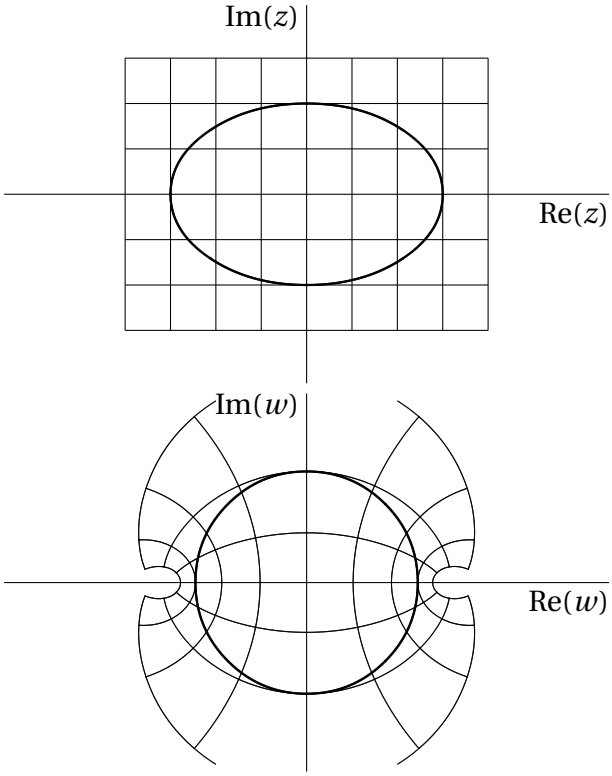

Figure 3.2: The conformal map.

Suppose that $R = \sqrt{ab}$. Then, using properties of the complete elliptic integral of the first kind and the Jacobi elliptic function [40],

$$w(z) \sim z - \frac{z^3}{4R^2}\, e^2 + O(e^4)\,. \tag{3.20}$$

Differentiating with respect to z,

$$w'(z) \sim 1 - \frac{3z^2}{4R^2}\, e^2 + O(e^4)\,. \tag{3.21}$$

Using the inverse of the conformal map (3.15), $z(w) \sim w + O(e^2)$, and with w in polar coordinates, $w = r\exp(i\theta)$,

$$|w'|^2 \sim 1 - \frac{3r^2\cos(2\theta)}{2R^2}\, e^2 + O(e^4)\,. \tag{3.22}$$

Now, let

$$\phi_m(w) \sim \phi_m^{(0)}(w) + \phi_m^{(2)}(w)\, e^2 + O(e^4)\,, \tag{3.23}$$

$$\lambda_m \sim \lambda_m^{(0)} + \lambda_m^{(2)}\, e^2 + O(e^4)\,. \tag{3.24}$$

At leading order, the field equation is

$$\left(\nabla^2 + (\lambda_m^{(0)})^2\right)\phi_m^{(0)}(w) = 0\,. \tag{3.25}$$

Using continuity, the eigenfunctions are

$$\phi_m^{(0)}(w) \propto \exp(im\theta)\,, \tag{3.26}$$

where m is an integer.

At next-to-leading order,

$$\left(\frac{3r^2\cos(2\theta)}{2R^2}\nabla^2 + 2\lambda_m^{(0)}\lambda_m^{(2)}\right)\phi_m^{(0)}(w) + \left(\nabla^2 + (\lambda_m^{(0)})^2\right)\phi_m^{(2)}(w) = 0\,. \tag{3.27}$$

Since the eigenfunctions $\phi_m^{(0)}$ are complete in the sense that

$$\phi_m^{(2)}(w) = \sum_{n\neq m} c_n \phi_n^{(0)}(w)\,, \tag{3.28}$$

equation (3.27) can be rewritten as

$$2\lambda_m^{(0)}\lambda_m^{(2)}\phi_m^{(0)}(w) = \frac{3r^2\cos(2\theta)}{2R^2}(\lambda_m^{(0)})^2\phi_m^{(0)}(w) + \sum_{n\neq m} c_n\big((\lambda_n^{(0)})^2 - \lambda_m^{(0)})^2\big)\phi_n^{(0)}(w)\,. \tag{3.29}$$

Multiplying both sides by $\exp(-im\theta)$ and integrating over θ from 0 to 2π, it follows that $\lambda_m^{(2)} = 0$. Therefore,

$$\lambda_m \sim \lambda_m^{(0)} + O(e^4)\,. \tag{3.30}$$

Since the eigenvalues do not change up to $O(e^4)$, the zero-point energy does not change up to $O(e^4)$ either; that is,

$$\mathscr{E}(a,e) \sim \mathscr{E}(R,0)\big(1+O(e^4)\big)\,, \tag{3.31}$$

Using $a = R(1-e^2)^{-1/4}$, the result from the zeta-function method is recovered.

3.2.3 Remarks

The major result of this section is equation (3.13). However, in many respects, equation (3.31) is more interesting. It states that the zero-point energy of the elliptical cylinder (3.1) is equal, up to $O(e^4)$, to that for a circular cylinder of radius $R = \sqrt{ab}$. Because R is the geometric mean of the semiaxes, it follows that the volume per unit longitudinal length of the circular cylinder is equal to that of the elliptical cylinder. This observation is recast as a conjecture:

> **Conjecture.** *Zero-point energy does not change for small deformations of the boundary that preserve volume.*

The conjecture is deliberately vague. In the present case it should be read as follows: (the change in the) zero-point energy (of a massless real scalar field subject to the Dirichlet condition on the boundary of an elliptical cylinder) does not change (up to $O(e^4)$) for small ($O(e^2)$) deformations of the boundary that preserve volume (per unit

longitudinal length). However, its vagueness allows the conjecture to be tested in other situations. For example, since only continuity is used in the conformal-map method, the conjecture is independent of the condition imposed on the boundary of an elliptical cylinder.

It should be mentioned that the conjecture can be restated in terms of small deformations of the boundary that preserve lateral surface area [47]. The two versions of the conjecture differ at the next-to-next-to-leading order in the eccentricity expansion. Unfortunately, calculating the zero-point energy beyond the next-to-leading order is considerably more difficult, and is not considered in this thesis. It may be that neither conjecture is valid beyond $O(e^2)$ deformations of the boundary.

3.3 Vector field

Quantizing the electromagnetic field is considerably more complicated than quantizing a massless real scalar field [34]. However, the result for the energy of the disturbed electromagnetic vacuum is very similar [32],

$$\langle 0|H|0\rangle_{\partial V} = \frac{1}{2}\sum_{\mathbf{k},\lambda}\omega_{\mathbf{k}}^{(\lambda)}. \tag{3.32}$$

The only difference is that the sum over the classical eigenenergies now includes the polarization states λ.

The classical Lagrangian density for the electromagnetic field is

$$\mathscr{L}_{\mathrm{EM}} = -\frac{1}{4}F_{\mu\nu}F^{\mu\nu}, \tag{3.33}$$

where $F_{\mu\nu} = \partial_\mu A_\nu - \partial_\nu A_\mu$. Applying the Euler-Lagrange equations, the field equations are

$$\partial_\mu F^{\mu\nu} = 0. \tag{3.34}$$

In terms of the electric and magnetic fields, $\mathbf{E} = -\nabla A^0 - \partial\mathbf{A}/\partial t$ and $\mathbf{B} = \nabla \times \mathbf{A}$ respectively, and with the time dependence given by $\exp(-i\omega t)$, the field equations (3.34)

become Maxwell's equations

$$\nabla \cdot \mathbf{E} = 0\,, \tag{3.35}$$

$$\nabla \cdot \mathbf{B} = 0\,, \tag{3.36}$$

$$\nabla \times \mathbf{E} = i\omega \mathbf{B}\,, \tag{3.37}$$

$$\nabla \times \mathbf{B} = -i\omega \mathbf{E}\,. \tag{3.38}$$

Perfectly-conducting conditions are given by $\mathbf{n} \times \mathbf{E} = \mathbf{0}$ and $\mathbf{n} \cdot \mathbf{B} = 0$ on the boundary, where $\mathbf{n}$ is the outward unit normal to the boundary. For the elliptical cylinder (3.1), the perfectly-conducting conditions become $E_v = 0$, $E_z = 0$ and $B_u = 0$ on the boundary $\cosh(u) = 1/e$.

Maxwell's equations are separable in elliptic-cylindrical coordinates [43]. There are two solutions, corresponding to the two polarization states. For the first solution, the general expression for the z component of the electric field in the interior of the boundary is

$$E_z^{\mathrm{I}} = \int \frac{dk}{2\pi} \exp(ikz) \Bigg(\sum_{m=0}^{\infty} A_m(k)\, \mathrm{Mc}_m^{(1)}(u,q)\, \mathrm{ce}_m(v,q) + \sum_{m=1}^{\infty} B_m(k)\, \mathrm{Ms}_m^{(1)}(u,q)\, \mathrm{se}_m(v,q) \Bigg). \tag{3.39}$$

This expression is identical to the general expression for a massless scalar field (3.5). Furthermore, the perfect-conducting boundary condition for this component, $E_z = 0$, is identical to the homogeneous Dirichlet condition. The boundary condition is satisfied when

$$\mathrm{Mc}_m^{(1)}(\operatorname{arccosh}(1/e), z^2 e^2/4) = 0\,, \tag{3.40}$$

$$\mathrm{Ms}_m^{(1)}(\operatorname{arccosh}(1/e), z^2 e^2/4) = 0\,, \tag{3.41}$$

where $z = \lambda a$ is a dimensionless variable. The other two boundary conditions are automatically satisfied because E_v^{I} and B_u^{I} each contain the same vanishing factors as E_z^{I}.

The second solution to Maxwell's equations follows from the principal of duality [48]. Now B_z^{I} has the general expression (3.39). Since $E_v^{\mathrm{I}} \propto \partial B_z^{\mathrm{I}}/\partial u$, the boundary condition

$E_v = 0$ is satisfied when

$$\mathrm{Mc}_m^{(1)\prime}(\operatorname{arccosh}(1/e), z^2e^2/4) = 0\,, \tag{3.42}$$

$$\mathrm{Ms}_m^{(1)\prime}(\operatorname{arccosh}(1/e), z^2e^2/4) = 0\,, \tag{3.43}$$

where $z = \lambda a$ and the prime denotes differentiation with respect to the first argument. The second solution is equivalent to a massless real scalar field subject to the homogeneous Neumann condition on the boundary.

The zero-point energy of the electromagnetic vacuum is given by the sum of the zero-point energies of the two polarization states. Since the two solutions are both equivalent to a massless real scalar field, and the first solution is subject to the Dirichlet condition on the boundary and the second solution is subject to the Neumann condition on the boundary,

$$\mathscr{E}(a,e) = \mathscr{E}^{\mathrm{D}}(a,e) + \mathscr{E}^{\mathrm{N}}(a,e)\,. \tag{3.44}$$

Using the fact that the eccentricity expansion of the zero-point energy does not depend on the boundary condition, the zero-point energy of the electromagnetic vacuum is

$$\mathscr{E}(a,e) \sim \mathscr{E}(a,0)\left(1 + \frac{1}{2}\,e^2 + O(e^4)\right), \tag{3.45}$$

where $\mathscr{E}(a,0) = \mathscr{E}^{\mathrm{D}}(a,0) + \mathscr{E}^{\mathrm{N}}(a,0)$. The prefactor $\mathscr{E}(a,0)$ is the zero-point energy of the electromagnetic field subject to perfectly-conducting conditions on the boundary of a cylinder of radius a (1.3).

Chapter 4

Spheroidal boundary

4.1 Introduction

In this chapter the boundary of a spheroidal is considered. Without any loss of generality, the boundary of a spheroidal can be given by $(x, y, z) \in \mathbb{R}^3$ such that

$$\frac{x^2}{a^2} + \frac{y^2 + z^2}{b^2} = 1\,, \tag{4.1}$$

where a and b are both nonzero. Figure 4.1 shows a prolate spheroid, for which $a > b$. Figure 4.2 shows an oblate spheroid, for which $a < b$.

The zero-point energy of an oblate spheroid can be formally obtained from that for a prolate spheroid; therefore, unless stated otherwise, the boundary is a prolate spheroid.

It is convenient to work in prolate-spheroidal coordinates. Using the notation in

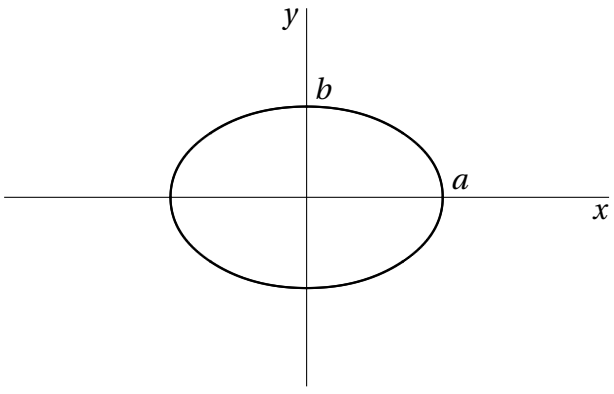

Figure 4.1: Rotating this ellipse about the x-axis yields a prolate spheroid.

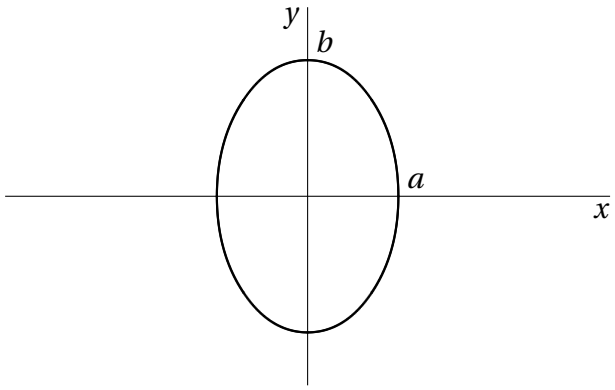

Figure 4.2: Rotating this ellipse about the x-axis yields an oblate spheroid.

Abramowitz and Stegun [40], prolate-spheroidal coordinates (ξ, η, φ) are related to Cartesian coordinates by

$$x = f\xi\eta\,, \tag{4.2}$$

$$y = f\sqrt{(\xi^2-1)(1-\eta^2)}\cos(\varphi)\,, \tag{4.3}$$

$$z = f\sqrt{(\xi^2-1)(1-\eta^2)}\sin(\varphi)\,, \tag{4.4}$$

where $f = \sqrt{a^2-b^2}$. The domains are $1 \le \xi < \infty$, $-1 \le \eta \le 1$ and $0 \le \varphi < 2\pi$. In prolate-spheroidal coordinates, the boundary (4.1) is given by

$$\xi = \frac{1}{e}\,, \tag{4.5}$$

where $e = f/a$ is the eccentricity.

As in the previous chapter, only small eccentricity is considered. The reason is the same: as the eccentricity tends to one, the boundary of the prolate spheroid becomes a circular cylinder, which is topologically different.

4.2 Scalar field

4.2.1 Zeta-function method

Consider a massless real scalar field that satisfies the homogeneous Dirichlet condition on the boundary of the prolate spheroid (4.1). Much of the following analysis is similar

to that for the elliptic-cylindrical boundary. The general expression for the field in the interior of the boundary is [35]

$$\phi^{\mathrm{I}} = \sum_{l=0}^{\infty} \sum_{m=-l}^{l} A_l^m \, \mathrm{S}_l^{m(1)}(\xi, \gamma^2) \, \mathrm{ps}_l^{m(1)}(\eta, \gamma^2) \exp(i m \varphi) \,, \tag{4.6}$$

where $\gamma = f\omega$, $\mathrm{ps}_l^{m(1)}$ are the angular prolate-spheroidal functions of the first kind and $\mathrm{S}_l^{m(1)}$ are the radial prolate-spheroidal functions of the first kind. Spheroidal functions are reviewed in appendix A.

The field satisfies the homogeneous Dirichlet condition on the boundary (4.1) when

$$\mathrm{S}_l^{m(1)}(1/e, z^2 e^2) = 0 \,, \tag{4.7}$$

where $z = \omega a$ is a dimensionless variable. The zeta function for this problem is

$$\zeta^{\mathrm{I,D}}(s, a, e) = (\mu a)^s \sum_{l=0}^{\infty} \sum_{m=-l}^{l} \frac{1}{2\pi i} \int_C dz \, z^{-s} \frac{\mathrm{S}_l^{m(1)\prime}(1/e, z^2 e^2)}{\mathrm{S}_l^{m(1)}(1/e, z^2 e^2)} \,. \tag{4.8}$$

Using the results in appendix A, the formal expansion of the integrand is

$$\begin{aligned} z^{-s} \frac{\mathrm{S}_l^{m(1)\prime}(1/e, z^2 e^2)}{\mathrm{S}_l^{m(1)}(1/e, z^2 e^2)} \sim z^{-s} \frac{\mathrm{j}_l'(z)}{\mathrm{j}_l(z)} - \frac{l^2 + l + m^2 - 1}{4l^2 + 4l - 3} \Bigg(s z^{-s} \frac{\mathrm{j}_l'(z)}{\mathrm{j}_l(z)} \\ + \left(z^{1-s} \frac{\mathrm{j}_l'(z)}{\mathrm{j}_l(z)} \right)' \Bigg) e^2 + O(e^4) \,, \end{aligned} \tag{4.9}$$

where the prime denotes differentiation with respect to z. The leading order reproduces the integrand for a spherical boundary of radius a. The first part of the next-to-leading term is proportional to the leading term. The second part of the next-to-leading term is continuous throughout C, has an antiderivative, and consequently, since the contour is closed, does not contribute to the zeta function. The contour integration is performed termwise. The leading term has no m dependence; the summation with respect to m of the leading term is $2l+1$. The prefactor of the next-to-leading term does depend on m. Using the relation,

$$\sum_{m=-l}^{l} \frac{l^2 + l + m^2 - 1}{4l^2 + 4l - 3} = \frac{2l+1}{3} \tag{4.10}$$

the formal expansion of the zeta function is

$$\zeta^{\mathrm{I,D}}(s, a, e) \sim \zeta^{\mathrm{I,D}}(s, a, 0) \left(1 - \frac{s}{3} e^2 + O(e^4) \right) . \tag{4.11}$$

By similar analysis, the result for the zeta function in the exterior of the boundary is

$$\zeta^{\mathrm{II,D}}(s,a,e) \sim \zeta^{\mathrm{II,D}}(s,a,0)\left(1-\frac{s}{3}\,e^2+O(e^4)\right). \tag{4.12}$$

The total zeta function is given by the sum of the internal and external contributions. Since the eccentricity expansion is the same in both regions,

$$\zeta^{\mathrm{D}}(s,a,e) \sim \zeta^{\mathrm{D}}(s,a,0)\left(1-\frac{s}{3}\,e^2+O(e^4)\right). \tag{4.13}$$

The prefactor is the total zeta function for a massless scalar field that satisfies the homogeneous Dirichlet condition on the boundary of a sphere of radius a, which can be shown to be well-behaved at $s=-1$ [30]. Using the principal-part prescription, the zero-point energy is

$$E^{\mathrm{D}}(a,e) \sim E^{\mathrm{D}}(a,0)\left(1+\frac{1}{3}\,e^2+O(e^4)\right). \tag{4.14}$$

This result is now confirmed using the Green-function method.

4.2.2 Green-function method

The reduced Green function for this problem, in the interior of the boundary, is [35]

$$\begin{aligned}\mathrm{g}^{\mathrm{I,D}}(\mathbf{x},\mathbf{x}') = -i\omega \sum_{l=0}^{\infty}\sum_{m=-l}^{l} &\mathrm{X}_l^m(\eta,\varphi,\gamma^2)\,\mathrm{X}_l^{m\,*}(\eta',\varphi',\gamma^2) \\ &\times \frac{\mathrm{S}_l^{m(3)}(1/e,\gamma^2)}{\mathrm{S}_l^{m(1)}(1/e,\gamma^2)}\,\mathrm{S}_l^{m(1)}(\xi,\gamma^2)\,\mathrm{S}_l^{m(1)}(\xi',\gamma^2)\,.\end{aligned} \tag{4.15}$$

where

$$\mathrm{X}_l^m(\eta,\varphi,\gamma^2) = \sqrt{\frac{2l+1}{4\pi}\frac{(l-m)!}{(l+m)!}}\,\mathrm{ps}_l^{m(1)}(\eta,\gamma^2)\exp(im\varphi)\,. \tag{4.16}$$

The reduced Green function in the exterior of the boundary is identical except that the radial prolate-spheroidal functions of the first and third kinds are interchanged.

The spatial integral is

$$\mathscr{I}(z,e) = \int d^3x\,\omega^2\,\mathrm{g}^{\mathrm{D}}(\mathbf{x},\mathbf{x})\,. \tag{4.17}$$

In prolate-spheroidal coordinates,

$$\mathscr{I}(z,e) = \int d\xi\, d\eta\, d\varphi\, f^3\big(\xi^2-\eta^2\big)\omega^2\, \mathrm{g}^{\mathrm{D}}(\mathbf{x},\mathbf{x})\,. \tag{4.18}$$

Using the reduced Green function, and scaling ξ by a factor of ze,

$$\begin{aligned}\mathscr{I}(z,e) = -i\sum_{l=0}^{\infty}\sum_{m=-l}^{l}\int_0^{2\pi} d\varphi \int_{-1}^{1} d\eta\, \mathrm{X}_l^m(\eta,\varphi,z^2e^2)\,\mathrm{X}_l^{m*}(\eta,\varphi,z^2e^2)\\ \times\Bigg(\frac{\mathrm{S}_l^{m(3)}(1/e,z^2e^2)}{\mathrm{S}_l^{m(1)}(1/e,z^2e^2)}\int_{ze}^{z} d\xi\,(\xi^2-\eta^2z^2e^2)\big(\mathrm{S}_l^{m(1)}(\xi,z^2e^2)\big)^2\\ +\frac{\mathrm{S}_l^{m(1)}(1/e,z^2e^2)}{\mathrm{S}_l^{m(3)}(1/e,z^2e^2)}\int_{z}^{\infty} d\xi\,(\xi^2-\eta^2z^2e^2)\big(\mathrm{S}_l^{m(3)}(\xi,z^2e^2)\big)^2\Bigg).\end{aligned} \tag{4.19}$$

The spatial integral is now expanded for small eccentricity,

$$\mathscr{I}(z,e) \sim \mathscr{I}^{(0)}(z) + \mathscr{I}^{(2)}(z)\,e^2 + O(e^4)\,. \tag{4.20}$$

The leading order term is simply the spatial integral for the same problem on the boundary of a sphere of radius a. The next-to-leading order term is given by

$$\mathscr{I}^{(2)}(z) = \lim_{e\to 0}\frac{1}{2!}\frac{\partial^2}{\partial e^2}\mathscr{I}(z,e)\,. \tag{4.21}$$

Because one of the integration limits depends on the eccentricity, Leibniz's rule is used. After simplifying,

$$\mathscr{I}^{(2)}(z) = \frac{1}{3}\mathscr{I}^{(0)}(z) - \frac{1}{3}\big(z\mathscr{I}^{(0)}(z)\big)'\,, \tag{4.22}$$

where the prime denotes differentiation with respect to z. When integrating over z, the total derivative vanishes. Effectively, the next-to-leading order term is equal to one-third the leading order term, which agrees with the result using the zeta-function method.

4.2.3 Remarks

Consider a sphere whose volume is equal to that of the prolate spheroid (4.1). The radius of the the sphere is $R = a(1-e^2)^{1/3}$. Substituting this into the result for the zero-point energy (4.14),

$$E^{\mathrm{D}}(a,e) \sim E^{\mathrm{D}}(R,0)\big(1+O(e^4)\big)\,. \tag{4.23}$$

In other words, the result in this section supports the conjecture that zero-point energy does not change for small deformations of the boundary that preserve volume.

The zero-point energy for an oblate-spheroidal boundary can be obtained using the following formal argument. Oblate eccentricity e' is formally related to prolate eccentricity by

$$\frac{1}{e^2} + \frac{1}{e'^2} = 1\,. \tag{4.24}$$

Substituting this relationship into the result for a prolate-spheroidal boundary, and expanding for small oblate eccentricity, yields

$$E^{\mathrm{D}}(a,e') \sim E^{\mathrm{D}}(a,0)\left(1 - \frac{1}{3}\,e'^2 + O(e'^4)\right). \tag{4.25}$$

This result for an oblate spheroidal boundary can be easily confirmed using the zeta-function and Green-function methods.

4.3 Vector field

The homogeneous vector Helmholtz differential equation is not separable in prolate-spheroidal coordinates [35]; the Robertson condition on the Stäckel determinant fails. Since solutions to Maxwell's equations also satisfy the homogeneous vector Helmholtz differential equation, it follows that Maxwell's equations are not separable in prolate-spheroidal coordinates. Consequently, the zeta-function and Green-function methods cannot be used to calculate the zero-point energy of the electromagnetic field subject to perfectly-conducting conditions on the boundary of a prolate spheroid.

There is, however, an exception: if the electromagnetic field is axially symmetric, then Maxwell's equations are separable in prolate-spheroidal coordinates [49]. In 2006, Kitson and Signal proposed that the zero-point energy could be obtained by suitably weighting the zeta function of the axially-symmetric, or zonal, components [50]. However, it is now shown that this zonal approximation is poor. The analysis is for a scalar field, for which the exact result is known and can therefore be compared with.

Recall that the zeta function for a massless real scalar field that satisfies the homogeneous Dirichlet condition on the boundary of a prolate spheroid is

$$\zeta^{\mathrm{I,D}}(s,a,e) = (\mu a)^s \sum_{l=0}^{\infty} \sum_{m=-l}^{l} \frac{1}{2\pi i} \int_C dz\, z^{-s} \frac{\mathrm{S}_l^{m(1)\prime}(1/e, z^2e^2)}{\mathrm{S}_l^{m(1)}(1/e, z^2e^2)}, \tag{4.26}$$

where $\mathrm{S}_l^{m(1)}$ are the radial prolate spheroidal functions of the first kind. Also recall that the formal eccentricity expansion of the integrand is

$$\begin{aligned} z^{-s} \frac{\mathrm{S}_l^{m(1)\prime}(1/e, z^2e^2)}{\mathrm{S}_l^{m(1)}(1/e, z^2e^2)} \sim z^{-s} \frac{\mathrm{j}_l'(z)}{\mathrm{j}_l(z)} - \frac{l^2+l+m^2-1}{4l^2+4l-3} \Bigg(s z^{-s} \frac{\mathrm{j}_l'(z)}{\mathrm{j}_l(z)} \\ + \left(z^{1-s} \frac{\mathrm{j}_l'(z)}{\mathrm{j}_l(z)} \right)' \Bigg) e^2 + O(e^4), \end{aligned} \tag{4.27}$$

where the prime denotes differentiation with respect to z. The zonal approximation is made by setting $m = 0$ in the integrand and replacing the summation with respect to m with 2ν, where $\nu = l + 1/2$. Let the zeta function for the zonal approximation be denoted by $\tilde{\zeta}$. For simplicity, set the mass scale μ equal to $1/a$. Suppose that the zeta function for the zonal approximation is expanded for small eccentricity

$$\tilde{\zeta}(s,a,e) \sim \tilde{\zeta}^{(0)}(s,a) + \tilde{\zeta}^{(2)}(s,a)\, e^2 + O(e^4). \tag{4.28}$$

At the leading order, the familiar zeta function for a spherical boundary is recovered,

$$\tilde{\zeta}^{(0)}(s,a) = \sum_{l=0}^{\infty} \frac{2\nu}{2\pi i} \int_C dz\, z^{-s} \frac{\mathrm{j}_l'(z)}{\mathrm{j}_l(z)}. \tag{4.29}$$

The Laurent expansion of the leading order about $s = -1$ is [51]

$$\tilde{\zeta}^{(2)}(s,a) = \frac{1}{315\pi} \frac{1}{s+1} - 0.00889\ldots + O(s+1). \tag{4.30}$$

At the next-to-leading order,

$$\tilde{\zeta}^{(2)}(s,a) = -s \sum_{l=0}^{\infty} \frac{5-4\nu^2}{16(1-\nu^2)} \frac{2\nu}{2\pi i} \int_C dz\, z^{-s} \frac{\mathrm{j}_l'(z)}{\mathrm{j}_l(z)}. \tag{4.31}$$

Continuing the contour integral to $-1 < \mathrm{Re}(s) < 0$,

$$\tilde{\zeta}^{(2)}(s,a) = -s \sum_{l=0}^{\infty} \frac{5-4\nu^2}{8(1-\nu^2)} \nu^{2-s} \frac{1}{\pi} \sin\left(\frac{\pi s}{2}\right) \int_0^{\infty} dy\, y^{-s} \left(\frac{1}{\nu} \frac{\mathrm{i}_l'(\nu y)}{\mathrm{i}_l(\nu y)} - 1 + \frac{1}{2\nu y} \right). \tag{4.32}$$

Then, continuing to a neighborhood of $s=-1$ and Laurent expanding,

$$\tilde{\zeta}^{(2)}(s,a)=\frac{3}{64\pi}\,\frac{1}{(s+1)^2}-\frac{2561-1890\,\gamma-5670\ln(2)}{40320\pi}\,\frac{1}{s+1}-0.03421\ldots+O(s+1)\,, \tag{4.33}$$

where $\gamma=0.57721\ldots$ is the Euler-Mascheroni constant.

The zero-point energy is obtained using the principal-part prescription. Factoring out the leading order,

$$\tilde{E}^{\mathrm{I,D}}(a,e)\sim\tilde{E}^{\mathrm{I,D}}(a,0)\big(1-3.85312\ldots e^2+O(e^4)\big)\,. \tag{4.34}$$

This does not compare well with the exact result,

$$E^{\mathrm{I,D}}(a,e)\sim E^{\mathrm{I,D}}(a,0)\big(1+0.25759\ldots e^2+O(e^4)\big)\,. \tag{4.35}$$

The next-to-leading-order term is not only of the wrong order of magnitude, but also has the wrong sign. In addition, the Laurent expansion of the zeta function for the zonal approximation contains a double pole, which contradicts the Poisson-kernel method. In conclusion, the zonal approximation is a poor approximation.

On the other hand, using the boundary-deformation conjecture,

$$E^{\mathrm{I,D}}(a,e)\sim E^{\mathrm{I,D}}(a,0)\left(1+\frac{1}{3}\,e^2+O(e^4)\right). \tag{4.36}$$

Comparing this with the exact result (4.35), the next-to-leading-order term has the correct sign and is of the right order of magnitude.

Chapter 5

Quantum chromodynamics

5.1 Introduction

Quantum chromodynamics, QCD for short, is the leading theory of the strong force. The theory describes how quark and gluon fields behave. QCD is a gauge theory with gauge group SU(3). Because the gauge group is non-Abelian, the field equations are highly nonlinear and, in general, too difficult to solve analytically.

The strong force has two particularly interesting properties. The first is asymptotic freedom: at high energies the coupling between the fields decreases. Asymptotic freedom can be derived from QCD [52, 53]. The other interesting property is confinement: at low energies, the coupling between the fields increases. One possible model for confinement is the dual-Meissner effect [54]. In electrodynamics, the Meissner effect is the expulsion of magnetic fields from superconductors. The dual of this is the expulsion of colour-electric fields, which forms flux tubes between coloured charges.

QCD is typically studied in one of three ways: perturbatively in the asymptotic freedom region, numerically on a lattice, or with models. One popular model is the MIT bag model, developed at the Massachusetts Institute of Technology [55, 56]. In the MIT bag model, hadrons, which are made up of quarks and gluons, are represented by bags. Inside the bag, the Lagrangian density for the MIT bag model is given by

$$\mathscr{L}_{\text{MIT}} = \mathscr{L}_{\text{QCD}} - B\,, \tag{5.1}$$

where $\mathscr{L}_{\text{QCD}}$ is the QCD Lagrangian density and B is the so-called bag constant. The

Lagrangian density for QCD is [32]

$$\mathscr{L}_{\mathrm{QCD}} = \sum_f \bar{\psi}_f \left(i\gamma^\mu D_\mu - m_f \right) \psi_f - \frac{1}{4} G^a_{\mu\nu} G^{a\mu\nu} . \tag{5.2}$$

Focusing on the first term, ψ_f are the quark fields, which come in six flavours, each with a different mass m_f; $\bar{\psi} = \psi^\dagger \gamma^0$, where the dagger denotes the Hermitian conjugate and γ^0 is one of the Dirac matrices γ^μ; and the covariant derivative

$$D_\mu = \partial_\mu + i g \frac{\lambda^a}{2} A^a_\mu , \tag{5.3}$$

where λ^a are the Gell-Mann matrices and A^a_μ are the eight massless gluon fields. The quark and the gluon fields are coupled together by g, which should not be confused with the reduced Green function. Focusing on the second term in the QCD Lagrangian density,

$$G^a_{\mu\nu} = \partial_\mu A^a_\nu - \partial_\nu A^a_\mu - g f^{abc} A^b_\mu A^c_\nu , \tag{5.4}$$

where the structure constants f^{abc} are related to the Gell-Mann matrices by the commutation relations

$$\left[\frac{\lambda^a}{2}, \frac{\lambda^b}{2} \right] = i f^{abc} \frac{\lambda^c}{2} . \tag{5.5}$$

It is assumed in the MIT bag model that the fields inside the bag can be treated perturbatively. In the zero-coupling limit, when $g = 0$, the field equation for the quarks reduces to the free Dirac equation

$$\left(i\gamma^\mu \partial_\mu - m \right) \psi = 0 , \tag{5.6}$$

subject to the condition $\left(1 + i\,\mathbf{n}\cdot\boldsymbol{\gamma}\right)\psi = 0$ on the boundary, where $\mathbf{n}$ is the unit outward normal. The field equations for the gluons become

$$\partial_\mu G^{\mu\nu}_a = 0 , \tag{5.7}$$

subject to the conditions $\mathbf{n}\cdot\mathbf{E}_a = 0$ and $\mathbf{n}\times\mathbf{B}_a = \mathbf{0}$ on the boundary. Because of the inclusion of the bag constant in the MIT Lagrangian, the fields are also subject to the

nonlinear condition

$$-\frac{1}{2}n^{\mu}\partial_{\mu}\bar{\psi}\psi-\frac{1}{4}G^{2}=B\,, \tag{5.8}$$

which is important for Lorentz invariance.

The total energy of a bag of volume V is [57]

$$E=E_{q}+E_{g}+BV\,, \tag{5.9}$$

where E_q is the contribution to the energy from the quarks and E_g is the contribution from the gluons. The bag constant stabilizes the bag; without the bag constant, the most favourable energy corresponds to a bag of infinite volume. Solving the model for a spherical bag of radius R, reasonable fits can be made to the masses of the lightest hadrons if an additional term of the form $-Z/R$, where $Z\sim 2$, is included in the total energy [57],

$$E'=E-\frac{Z}{R}\,. \tag{5.10}$$

About half of Z can be accounted for by centre-of-mass corrections [58]; the possibility that the other half can be explained by zero-point energy has been considered by many authors.

5.2 Spherical bag

In 1976, Bender and Hays calculated the zero-point energies of massless quarks and gluons in the zero-coupling limit of the MIT bag model for a spherical bag [59]. Because there are no external fields in the MIT bag model, they found that the zero-point energies are divergent.

In 1980, Milton used the Green-function method to calculate the zero-point energies beyond the leading divergence [16, 17, 60]. Milton argued that the divergent terms can be renormalized by adding additional phenomenological terms to the total energy

of the bag (5.10). If the divergent terms are renormalized, then the remaining finite part is

$$E \sim \frac{0.7}{R}\,, \tag{5.11}$$

where R is the radius of the bag. A similar result was also obtained by Romeo using the zeta-function method [61]. While the contribution to Z is of the correct order of magnitude, it is of the wrong sign.

It is perhaps not surprising that the calculated value for Z in the zero-coupling limit does not agree with the value from the mass fits. This is because the mass fits suggest that the coupling is large, $g \sim 2$, which implies that nonperturbative effects are important. Recently, some progress has been made in including some of the nonperturbative behaviour. In 2005 Oxman *et al.* considered modifying the reduced Green function [62]. The following is a simplification of their argument; for full details see their paper.

Referring to studies of the Schwinger-Dyson equation, Oxman *et al.* consider the following modified reduced Green-function,

$$\tilde{\mathrm{g}}(k^2) = \frac{(-k^2)^\lambda}{(-k^2+\Lambda^2)^{\lambda+1}}\,, \tag{5.12}$$

where k^μ is momentum, $\Lambda = O(\Lambda_{\mathrm{QCD}})$ and $\lambda > 0$. For large k^2, the modified reduced Green function reduces to $\mathrm{g}(k^2) = -1/k^2$, which is the unmodified reduced Green function. However, the small k^2 behaviour is very different, $\mathrm{g}(k^2) \sim (-k^2)^\lambda$. The modified reduced Green function can be written in terms of the unmodified reduced Green function,

$$\tilde{\mathrm{g}}(k^2) = \mathrm{g}(k^2)^{-\lambda}\,\mathrm{g}(k^2-\Lambda^2)^{\lambda+1}\,. \tag{5.13}$$

Using Cauchy's theorem, it is straightforward to show that zero-point energy can be given by

$$E = -\frac{1}{2}\sum_{\mathbf{k}}\frac{1}{2\pi i}\int d\omega\,\ln\left(\mathrm{g}(\omega^2-\omega_{\mathbf{k}}^2)\right), \tag{5.14}$$

where **k** is an index. Replacing the unmodified reduced Green function with the modified one, expanding the logarithm and integrating termwise,

$$\tilde{E} = -\lambda E(0) + (\lambda + 1)E(\Lambda^2)\,, \tag{5.15}$$

where E is the zero-point energy for the unmodified reduced Green function. The second term corresponds to the zero-point energy for the field with mass Λ, which is assumed to be small. Neglecting the second term,

$$\tilde{E} \sim -\lambda E(0)\,. \tag{5.16}$$

Using Milton's result (5.11) and $\lambda \sim 1$, which corresponds to a typical value in the Schwinger-Dyson studies,

$$\tilde{E} \sim -\frac{0.7}{R}\,. \tag{5.17}$$

The crucial minus sign implies that the calculated zero-point energy now agrees with the mass fits.

5.3 Spheroidal bag

Lattice QCD is the numerical study of QCD on a finite lattice. The finite spacing between the lattice points acts as the regulating cutoff. As the lattice becomes finer, the approximation to QCD becomes better. Because of the complexity of the underlying QCD field equations, lattices are small, typically of the order of $16^3 \times 32$, and even then calculations require supercomputers.

However, with the ever-increasing power of computing, dramatic pictures of the QCD vacuum are starting to emerge. The figures in this chapter are used with the kind permission of Derek Leinweber; they are a series of stills from animations that can be found on his website [63]. Figure 5.1 shows a lattice simulation of a meson. The depression in the sheet represents the reduction of the vacuum action. The flux tube joining the quark and antiquark is the region of space where the vacuum is maximally expelled.

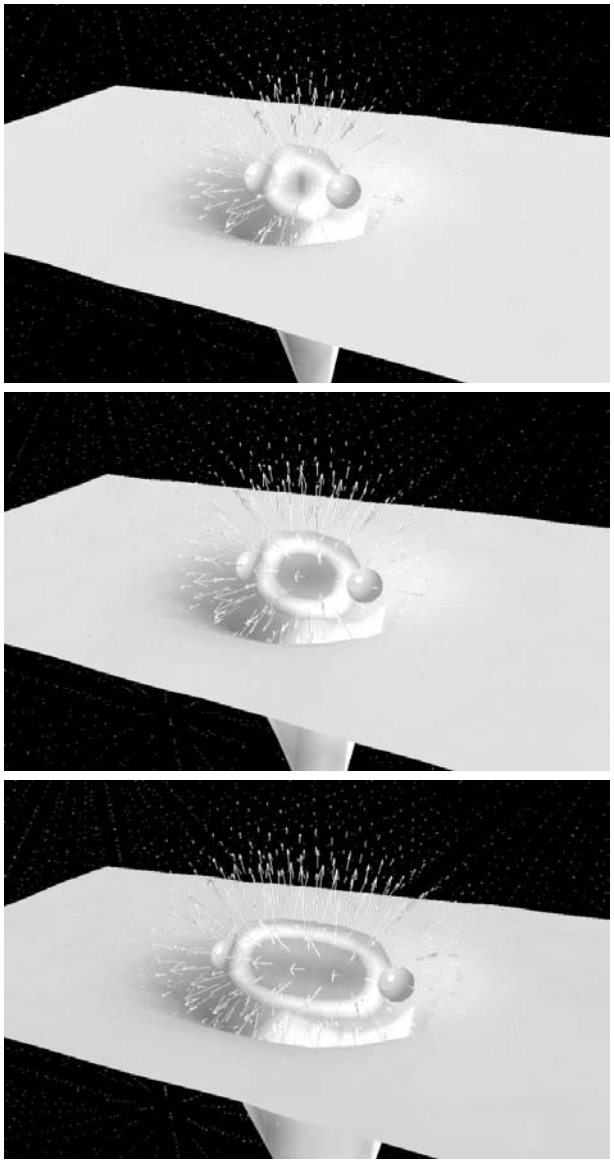

Figure 5.1: Lattice simulation of a meson.

This simulation is artificial in the sense that dynamical quarks are not included. If dynamical quarks are included, then separating the quark and antiquark eventually introduces so much energy that the hadron splits, forming new hadrons in a process known as hadronization. Consequently, in the following analysis, only small separations are considered.

For small separations, the flux tube can be modeled by a prolate spheroid. A small increase in the separation corresponds to a small increase in the eccentricity while holding the semiminor axis b fixed. The zero-point energy of this flux tube is now considered. Assuming the boundary-deformation conjecture, and using the modified Green function result for the spherical bag (5.17), the zero-point energy for a prolate-spheroidal bag is

$$E \sim -\frac{0.7}{a}\left(1+\frac{1}{3}\,e^2+O(e^4)\right). \tag{5.18}$$

Using the relationship between a and b, $a = b(1-e^2)^{-1/2}$,

$$E \sim -\frac{0.7}{b}\left(1-\frac{1}{6}\,e^2+O(e^4)\right). \tag{5.19}$$

With b fixed, the energy increases as the eccentricity increases.

Figure 5.2 shows a lattice simulation of a baryon. For small separations of the three quarks, the flux tube can be modeled by an oblate spheroid. A small increase in the separation corresponds to a small increase in the oblate eccentricity while holding the semiminor axis a fixed. The zero-point energy for an oblate-spheroidal bag is

$$E \sim -\frac{0.7}{a}\left(1-\frac{1}{3}\,e'^2+O(e'^4)\right). \tag{5.20}$$

With a fixed, the energy increases as the oblate eccentricity increases.

Both results imply that a spherical bag is most stable; deforming a spherical bag into either a prolate or oblate spheroidal bag results in an increase in the energy. The results are also consistent with results that show that the energy per unit length of the flux tube is constant [64].

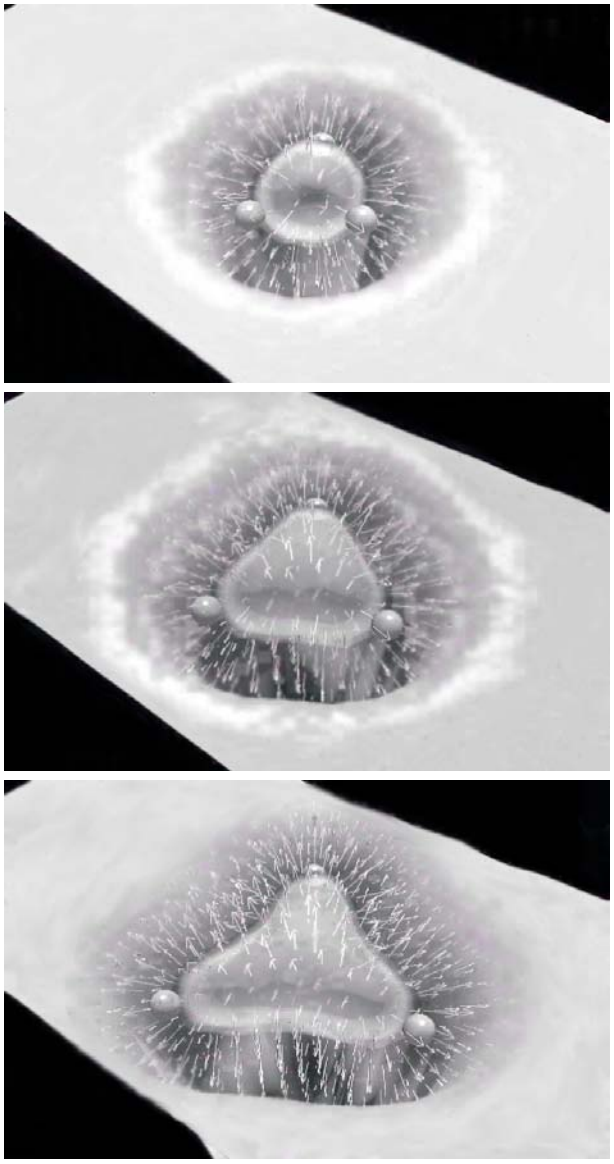

Figure 5.2: Lattice simulation of a baryon.

Chapter 6

Conclusion

In chapter 3, the zero-point energy of an elliptic-cylindrical boundary was considered. Using the zeta-function method, the zero-point energy of a massless real scalar field was evaluated in a formal series in terms of small eccentricity. The result was confirmed using a method that used a conformal map to map the problem onto the simpler problem of a circular cylinder. The result for the zero-point energy led to the conjecture that zero-point energy does not change for small deformations of the boundary that preserve volume. Because no boundary condition other than continuity was used in the conformal-map method, the conjecture is independent of the condition imposed on the field on the boundary of the elliptical cylinder. The zero-point energy of a vector field was also considered. It was shown that the zero-point energy for the vector field reduced to the sum of the zero-point energies of two scalar fields satisfying different conditions on the boundary. Since the boundary-deformation conjecture is independent of the boundary condition, and therefore the eccentricity expansion is independent of the boundary condition, the result for the vector field was obtained immediately.

In chapter 4, the zero-point energy of a spheroidal boundary was considered. Again, the zeta-function method was used to evaluate the zero-point energy of a massless real scalar field, and again the result was expanded in a formal series in terms of small eccentricity. The result was confirmed using the Green-function method. The result for the zero-point energy supported the boundary-deformation conjecture. No exact result was obtained for the zero-point energy of a vector field because the field equations

are not separable in spheroidal coordinates.

The spheroidal boundary was considered again in chapter 5, where it was used to model flux tubes between quarks in hadrons. Assuming the boundary-deformation conjecture, it was found that the zero-point energy of the flux tubes increases as the quarks are separated, and therefore zero-point energy plays a stabilizing role in quantum chromodynamics.

The work in this thesis could be extended in many ways. For example, the boundary-deformation conjecture could be tested by calculating the next term in the eccentricity expansion. Or perhaps the Poisson-kernel method, with its strong connection with geometry, could be used to study the conjecture theoretically. The conjecture could also be tested for spinor fields and fields with mass.

It is tempting to relate the work in this thesis with the work of Ambjørn and Wolfram on cuboidal boxes [19]. However, their results, showing the change in the zero-point energy as a cubic box is deformed into a cuboid, are only calculated for the field inside the box, and therefore dependent on the renormalization method. The method they use is the zeta-function method, which hides the fact that their results are technically divergent. Neglecting the divergent part, as Ambjørn and Wolfram do, the results show the zero-point energy changing sign as the cubic box is deformed. A result such as this for a boundary whose zero-point energy can be calculated unambiguously, such as spheroids, would be of considerable interest.

Appendix A

Mathieu and spheroidal functions

A.1 Mathieu functions

A.1.1 Separation of variables

In elliptic-cylindrical coordinates (u, v, z), the scalar Helmholtz differential equation is

$$\left(\frac{2}{f^2(\cosh(2u)-\cos(2v))}\left(\frac{\partial^2}{\partial u^2}+\frac{\partial^2}{\partial v^2}\right)+\frac{\partial^2}{\partial z^2}+\omega^2\right)\phi=0\,, \tag{A.1}$$

where $f=\sqrt{a^2-b^2}$. The semimajor axis a is greater than the semiminor axis b, and both are nonzero. Suppose that $\phi=\mathrm{U}(u)\mathrm{V}(v)\mathrm{Z}(z)$. Then, Z satisfies the differential equation

$$\left(\frac{d^2}{dz^2}+k^2\right)\mathrm{Z}=0\,, \tag{A.2}$$

where k is a separation constant. The equations for U and V are, respectively,

$$\left(\frac{d^2}{du^2}-a+2q\cosh(2u)\right)\mathrm{U}=0\,, \tag{A.3}$$

$$\left(\frac{d^2}{dv^2}+a-2q\cos(2v)\right)\mathrm{V}=0\,, \tag{A.4}$$

where $q=f^2\lambda^2$, $\lambda^2=\omega^2-k^2$, and a, which should not be confused with the semimajor axis, is another separation constant. In general, a depends on q and another parameter m; this is written $a_m(q)$. Solutions to equation (A.3) are the modified Mathieu functions; solutions to equation (A.4) are the Mathieu functions.

A.1.2 Mathieu functions

For the field ϕ to be continuous, it is necessary that the solutions to equation (A.4) are periodic with respect to v. The periodic solutions are often separated into those that are even with respect to v and those that are odd. The even periodic Mathieu functions are denoted by ce_m. They are normalized such that

$$\frac{1}{\pi}\int_0^{2\pi} dv\, \mathrm{ce}_m(v,q)\,\mathrm{ce}_{m'}(v,q) = \delta_{mm'}\,, \tag{A.5}$$

where δ is the Kronecker delta. The odd Mathieu functions are denoted by se_m and are normalized in a similar fashion.

In this thesis, the behaviour of the Mathieu functions for small q is of interest, as this corresponds to small eccentricity. This behaviour is studied by formally expanding the Mathieu functions in terms of q.

Consider the even Mathieu function ce_0. Suppose that

$$\mathrm{ce}_0(v,q) \sim \mathrm{ce}_0^{(0)}(v) + \mathrm{ce}_0^{(1)}(v)\,q + O(q^2)\,, \tag{A.6}$$

$$a_0(q) \sim a_0^{(0)} + a_0^{(1)}\,q + O(q^2)\,. \tag{A.7}$$

At leading order, it is easy to show that $a_0^{(0)} = 0$ and, after normalizing, $\mathrm{ce}_0^{(0)}(v) = 1/\sqrt{2}$.

At next-to-leading order, the Mathieu differential equation (A.4) implies that

$$\mathrm{ce}_0^{(1)\prime\prime}(v) + \frac{a_0^{(1)}}{\sqrt{2}} - \sqrt{2}\cos(2v) = 0\,, \tag{A.8}$$

where the primes denote differentiation with respect to v. The general solution to equation (A.8) is

$$\mathrm{ce}_0^{(1)}(v) = c_0 + c_1 v - \frac{a_0^{(1)}}{2\sqrt{2}}v^2 - \frac{\cos(2v)}{2\sqrt{2}}\,, \tag{A.9}$$

where c_0 and c_1 are arbitrary constants. Since ce_0 is periodic, c_1 and $a_0^{(1)}$ must be zero. The normalization condition (A.5) implies that c_0 is zero. Therefore,

$$\mathrm{ce}_0(v,q) \sim \frac{1}{\sqrt{2}}\left(1 - \frac{1}{2}\cos(2v)\,q + O(q^2)\right). \tag{A.10}$$

Similarly,

$$\mathrm{ce}_1(v,q) \sim \cos(v) - \frac{1}{8}\cos(3v)\, q + O(q^2) \tag{A.11}$$

and, for $m > 1$,

$$\mathrm{ce}_m(v,q) \sim \cos(mv) + \frac{(m+1)\cos((m-2)v) - (m-1)\cos((m+2)v)}{4(m^2-1)}\, q + O(q^2)\,. \tag{A.12}$$

The analysis for the odd Mathieu functions is similar. The results are

$$\mathrm{se}_1(v,q) \sim \sin(v) - \frac{1}{8}\sin(3v)\, q + O(q^2) \tag{A.13}$$

and, for $m > 1$,

$$\mathrm{se}_m(v,q) \sim \sin(mv) + \frac{(m+1)\sin((m-2)v) - (m-1)\sin((m+2)v)}{4(m^2-1)}\, q + O(q^2)\,. \tag{A.14}$$

There is no odd Mathieu function for $m = 0$.

A.1.3 Modified Mathieu functions

There are four kinds of modified Mathieu functions. Only the first and third kinds inplies the correct behaviour to the field ϕ at the origin and infinity, respectively [65]. The even modified Mathieu functions of the first kind are denoted $\mathrm{Mc}_m^{(1)}$. They are normalized such that, for large $u' = 2\sqrt{q}\cosh(u)$,

$$\mathrm{Mc}_m^{(1)}(u,q) \sim \mathrm{J}_m(u')\,, \tag{A.15}$$

where J_m are the Bessel functions of the first kind. The odd modified Mathieu functions are denoted by $\mathrm{Ms}_m^{(1)}$ and are normalized in a similar fashion.

Consider the even modified Mathieu function of the first kind $\mathrm{Mc}_0^{(1)}$. Solving equation (A.3) formally in terms of q while holding u' fixed, and using the result from the previous subsection that $a_0(q) \sim O(q^2)$,

$$\mathrm{Mc}_0^{(1)}(u,q) \sim \mathrm{J}_0(u') + \frac{\mathrm{J}_1(u')}{u'}\, q + O(q^2)\,. \tag{A.16}$$

Making the substitutions $u = \operatorname{arccosh}(1/e)$ and $q = z^2 e^2/4$ gives the formal eccentricity expansion

$$\mathrm{Mc}_0^{(1)}(\operatorname{arccosh}(1/e), z^2 e^2/4) \sim \mathrm{J}_0(z) + \frac{z}{4}\mathrm{J}_1(z)\, e^2 + O(e^4)\,. \tag{A.17}$$

Similarly, for $m > 0$,

$$\mathrm{Mc}_m^{(1)}(\operatorname{arccosh}(1/e), z^2 e^2/4) \sim \mathrm{J}_m(z) - \frac{z}{4}\left(\mathrm{J}'_m(z) - \frac{\delta_{m1}}{2}\mathrm{J}_0(z)\right) e^2 + O(e^4)\,, \tag{A.18}$$

where the prime denotes differentiation with respect to z, and δ is the Kronecker delta.

The analysis for the odd modified Mathieu functions of the first kind is similar. For $m > 0$,

$$\mathrm{Ms}_m^{(1)}(\operatorname{arccosh}(1/e), z^2 e^2/4) \sim \mathrm{J}_m(z) - \frac{z}{4}\left(\mathrm{J}'_m(z) + \frac{\delta_{m1}}{2}\mathrm{J}_0(z)\right) e^2 + O(e^4)\,. \tag{A.19}$$

There is no odd modified Mathieu function for $m = 0$.

Figure A.1 shows $\mathrm{Mc}_0^{(1)}$ and its formal eccentricity expansion up to $O(e^4)$ for several values of z. It can be seen that the eccentricity expansion is reasonably good for small eccentricity, and best for small z. This trend holds for the other even and odd modified Mathieu functions.

The even and odd modified Mathieu functions of the third kind are denoted by $\mathrm{Mc}_m^{(3)}$ and $\mathrm{Ms}_m^{(3)}$, respectively. Their eccentricity expansions are identical to those of the first kind except that Bessel functions of the first kind are replaced with Hankel functions of the first kind.

A.2 Spheroidal functions

A.2.1 Separation of variables

The scalar Helmholtz differential equation is separable in both prolate-spheroidal and oblate-spheroidal coordinates. Since oblate-spheroidal functions can be expressed

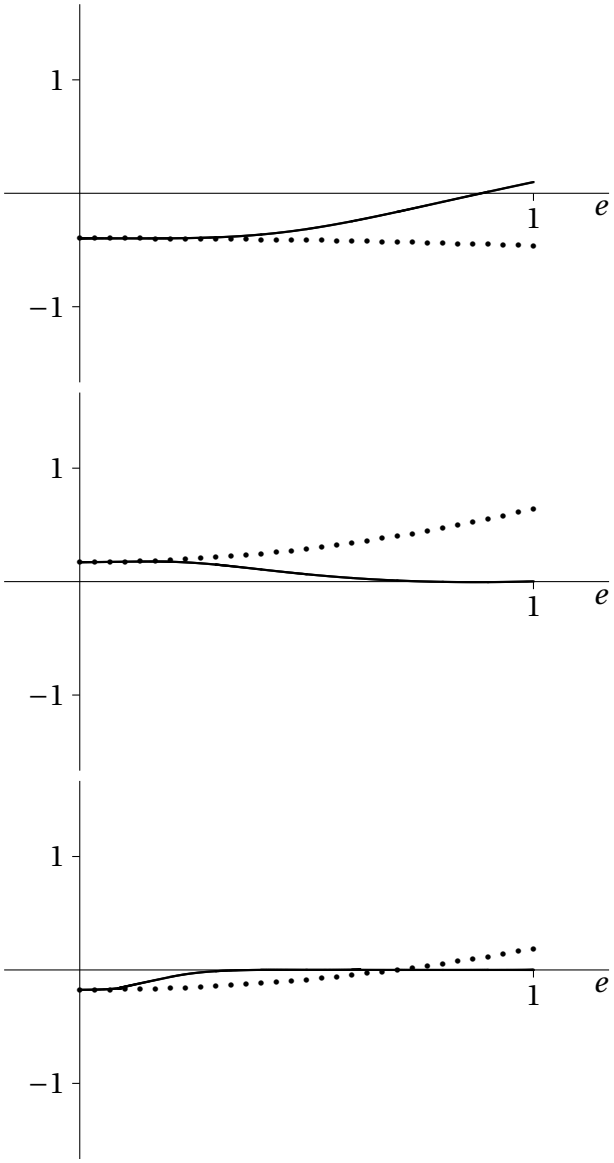

Figure A.1: These three plots compare the modified Mathieu function Mc_0, the solid line, with its formal eccentricity expansion up to $O(e^4)$, the dotted line. From top to bottom, z is 4, 8 and 16.

in terms of prolate-spheroidal functions [40], only prolate-spheroidal coordinates are considered here.

Suppose that $\phi = \Xi(\xi)\,\mathrm{H}(\eta)\Phi(\varphi)$, where (ξ,η,φ) are prolate-spheroidal coordinates. It follows from the scalar Helmholtz differential equation that the equation for Φ is

$$\left(\frac{d^2}{d\varphi^2} + m^2\right)\Phi = 0\,, \tag{A.20}$$

where m is a separation constant. For the field ϕ to be continuous, it is necessary that Φ is periodic with respect to φ. Suitable solutions for Φ are $\exp(im\varphi)$, where m is an integer. The equations for Ξ and H are, respectively,

$$\left((\xi^2-1)\frac{d^2}{d\xi^2} + 2\xi\frac{d}{d\xi} - \lambda_{lm}(\gamma^2) + \gamma^2(\xi^2-1) - \frac{m^2}{\xi^2-1}\right)\Xi = 0\,, \tag{A.21}$$

$$\left((1-\eta^2)\frac{d^2}{d\eta^2} - 2\eta\frac{d}{d\eta} + \lambda_{lm}(\gamma^2) - \gamma^2(1-\eta^2) - \frac{m^2}{1-\eta^2}\right)\mathrm{H} = 0\,, \tag{A.22}$$

where $\gamma = f\omega$, and λ is another separation constant. Solutions to equation (A.21) are the radial prolate-spheroidal functions; solutions to equation (A.22) are the angular prolate-spheroidal functions.

A.2.2 Angular prolate-spheroidal functions

There are two kinds of angular prolate-spheroidal functions. Only the first kind are considered here, as only the first kind are well-behaved at $\eta = -1$ and $\eta = 1$ [40]. The angular prolate-spheroidal functions of the first kind are denoted $\mathrm{ps}_l^{m\,(1)}$. Here l is a positive integer such that $|m| \le l$. There are several normalization schemes for the angular prolate-spheroidal functions; the normalization used in this thesis is the Meixner and Schäfka normalization [65],

$$\int_{-1}^{1} d\eta\, \mathrm{ps}_l^{m\,(1)}(\eta,\gamma^2)\,\mathrm{ps}_{l'}^{m\,(1)}(\eta,\gamma^2) = \frac{2}{2l+1}\frac{(l+m)!}{(l-m)!}\delta_{ll'}\,. \tag{A.23}$$

Formally expanding for small γ^2,

$$\begin{aligned}\mathrm{ps}_l^{m\,(1)}(\eta,\gamma^2) \sim \mathrm{P}_l^m(\eta) + \Bigg(&\frac{(l+m-1)(l+m)}{2(2l-1)^2(2l+1)}\,\mathrm{P}_{l-2}^m(\eta)) \\ &- \frac{(l-m+1)(l-m+2)}{2(2l+1)(2l+3)^2}\,\mathrm{P}_{l+2}^m(\eta)\Bigg)\gamma^2 + O(\gamma^4)\,.\end{aligned} \tag{A.24}$$

where P_l^m are the associated Legendre functions of type I.

A.2.3 Radial prolate-spheroidal functions.

As for the modified Mathieu functions, there are four kinds of radial prolate-spheroidal functions. Only the first and third kinds are of interest in this thesis. The radial prolate-spheroidal functions of the first kind are denoted $\mathrm{S}_l^{m\,(1)}$. They are normalized such that, for large $\gamma\xi$,

$$\mathrm{S}_l^{m\,(1)}(\xi,\gamma^2) \sim \mathrm{j}_l(\gamma\xi)\,, \tag{A.25}$$

where j_l are the spherical Bessel functions of the first kind.

Formally expanding for small eccentricity,

$$\mathrm{S}_l^{m\,(1)}(1/e, z^2e^2) \sim \mathrm{j}_l(z) - \left(\frac{l^2+l+m^2-1}{4l^2+4l-3}\, z\mathrm{j}_l'(z) - \frac{l^2+l-3m^2}{8l^2+8l-6}\,\mathrm{j}_l(z)\right)e^2 + O(e^4)\,. \tag{A.26}$$

The eccentricity expansion of the radial prolate-spheroidal functions of the third kind $\mathrm{S}_l^{m\,(3)}$ is identical to that of the first kind except that spherical Bessel functions of the first kind are replaced with spherical Hankel functions of the first kind.

Bibliography

[1] H. B. G. Casimir, On the attraction between two perfectly conducting plates, Kon. Ned. Akad. Wetensch. Proc. **51**, 793 (1948).

[2] M. J. Sparnaay, Measurements of attractive forces between flat plates, Physica **24**, 751 (1958).

[3] S. K. Lamoreaux, Demonstration of the Casimir force in the 0.6 to 6μm range, Phys. Rev. Lett. **78**, 5 (1997), Erratum, ibid **81**, 5475 (1998).

[4] U. Mohideen and A. Roy, Precision measurement of the Casimir force from 0.1 to 0.9μm, Phys. Rev. Lett. **81**, 4549 (1998), physics/9805038.

[5] A. Roy, C.-Y. Lin, and U. Mohideen, Improved precision measurement of the Casimir force, Phys. Rev. D **60**, 111101 (1999), quant-ph/9906062.

[6] J. Blocki, J. Randrup, W. J. Swiatecki, and C. F. Tsang, Proximity forces, Ann. Phys. **105**, 427 (1977).

[7] G. Bressi, G. Carugno, R. Onofrio, and G. Ruoso, Measurement of the Casimir force between parallel metallic surfaces, Phys. Rev. Lett. **88**, 041804 (2002), quant-ph/0203002.

[8] M. Bordag, U. Mohideen, and V. M. Mostepanenko, New developments in the Casimir effect, Phys. Rept. **353**, 1 (2001), quant-ph/0106045.

[9] S. K. Lamoreaux, The Casimir force: background, experiments, and applications, Rep. Prog. Phys. **68**, 201 (2005).

[10] M. Bordag, D. Hennig, and D. Robaschik, Vacuum energy in quantum field theory with external potentials concentrated on planes, J. Phys. A: Math. Gen. **25**, 4483 (1992).

[11] M. Bordag, K. Kirsten, and D. Vassilevich, Ground state energy for a penetrable sphere and for a dielectric ball, Phys. Rev. **D59**, 085011 (1999), hep-th/9811015.

[12] N. Graham *et al.*, Calculating vacuum energies in renormalizable quantum field theories: a new approach to the Casimir problem, Nucl. Phys. **B645**, 49 (2002), hep-th/0207120.

[13] N. Graham *et al.*, Casimir energies in light of quantum field theory, Phys. Lett. **B572**, 196 (2003), hep-th/0207205.

[14] N. Graham *et al.*, The Dirichlet Casimir problem, Nucl. Phys. **B677**, 379 (2004).

[15] E. M. Lifshitz, The theory of molecular attractive forces between solids, Soviet Phys. JEPT **2**, 73 (1956).

[16] K. A. Milton, Zero-point energy in bag models, Phys. Rev. **D22**, 1441 (1980).

[17] K. A. Milton, Zero-point energy of confined fermions, Phys. Rev. **D22**, 1444 (1980), Erratum, ibid **D25**, 3441 (1982).

[18] P. Hays, Vacuum fluctuations of a confined massive field in two dimensions, Ann. Phys. **121**, 32 (1979).

[19] J. Ambjørn and S. Wolfram, Properties of the vacuum. 1. Mechanical and thermodynamic, Ann. Phys. **147**, 1 (1983).

[20] C. M. Bender and K. A. Milton, Casimir effect for a D-dimensional sphere, Phys. Rev. **D50**, 6547 (1994), hep-th/9406048.

[21] K. A. Milton, Vector Casimir effect for a D-dimensional sphere, Phys. Rev. **D55**, 4940 (1997), hep-th/9611078.

[22] E. Sassaroli, Y. N. Srivastava, and A. Widom, Photon production by the dynamical Casimir effect, Phys. Rev. **A50**, 1027 (1994).

[23] K. A. Milton, *The Casimir Effect: Physical Manifestations of Zero-Point Energy* (World Scientific, 2001).

[24] D. Deutsch and P. Candelas, Boundary effects in quantum field theory, Phys. Rev. **D20**, 3063 (1979).

[25] H. B. G. Casimir, Introductory remarks on quantum electrodynamics, Physica **19**, 846 (1956).

[26] T. H. Boyer, Quantum electromagnetic zero point energy of a conducting spherical shell and the Casimir model for a charged particle, Phys. Rev. **174**, 1764 (1968).

[27] B. Davies, Quantum electromagnetic zero-point energy of a conducting spherical shell, J. Math. Phys. **13**, 1324 (1972).

[28] R. Balian and B. Duplantier, Electromagnetic waves near perfect conductors. II. Casimir effect, Ann. Phys. **112**, 165 (1978).

[29] K. A. Milton, L. L. DeRaad, Jr., and J. S. Schwinger, Casimir self-stress on a perfectly conducting spherical shell, Ann. Phys. **115**, 388 (1978).

[30] S. Leseduarte and A. Romeo, Complete zeta-function approach to the electromagnetic Casimir effect for spheres and circles, Ann. Phys. **250**, 448 (1996), hep-th/9605022.

[31] L. L. DeRaad, Jr. and K. A. Milton, Casimir self-stress on a perfectly conducting cylindrical shell, Ann. Phys. **136**, 229 (1981).

[32] G. Plunien, B. Muller, and W. Greiner, The Casimir effect, Phys. Rept. **134**, 87 (1986).

[33] E. T. Whittaker and G. N. Watson, *A Course of Modern Analysis* (Cambridge University Press, 1962).

[34] C. Itzykson and J.-B. Zuber, *Quantum Field Theory* (McGraw-Hill, 1980).

[35] P. M. Morse and H. Feshbach, *Methods of Theoretical Physics* (McGraw-Hill, 1953).

[36] L. S. Brown and G. J. Maclay, Vacuum stress between conducting plates: An image solution, Phys. Rev. **184**, 1272 (1969).

[37] R. L. Jaffe and A. Scardicchio, Casimir effect and geometric optics, Phys. Rev. Lett. **92**, 070402 (2004), quant-ph/0509071.

[38] S. Blau, M. Visser, and A. Wipf, Zeta functions and the Casimir energy, Nucl. Phys. **B310**, 163 (1988).

[39] S. A. Fulling, Vacuum energy as spectral geometry, SIGMA **3** (2007), math-th/0706.2831.

[40] M. Abramowitz and I. A. Stegun, editors, *Handbook of Mathematical Functions* (Dover Publications, 1972).

[41] S. Leseduarte and A. Romeo, Zeta function of the bessel operator on the negative real axis, J. Phys. A: Math. Gen. **27**, 2483 (1994).

[42] P. Gosdzinsky and A. Romeo, Energy of the vacuum with a perfectly conducting and infinite cylindrical surface, Phys. Lett. **B441**, 265 (1998), hep-th/9809199.

[43] N. W. McLachlan, *Theory and Application of Mathieu Functions* (Clarendon Press, 1947).

[44] A. A. Kvitsinsky, Zeta functions of nearly circular domains, J. Phys. A: Math. Gen. **29**, 6379 (1996).

[45] A. R. Kitson and A. Romeo, Perturbative zero-point energy for a cylinder of elliptical section, Phys. Rev. **D74**, 085024 (2006), hep-th/0607206.

[46] H. Kober, *Dictionary of Conformal Representations* (Dover Publications, 1957).

[47] A. Romeo, private communication (2006).

[48] J. D. Jackson, *Classical Electrodynamics*, Third ed. (Wiley, 1998).

[49] L. Page, The electrical oscillations of a prolate spheroid. Paper II prolate spheroidal wave functions, Phys. Rev. **65**, 98 (1944).

[50] A. R. Kitson and A. I. Signal, Zero-point energy in spheroidal geometries, J. Phys. **A39**, 6473 (2006), hep-th/0511048.

[51] A. Romeo, Bessel ζ-function approach to the Casimir effect of a scalar field in a spherical bag, Phys. Rev. **D52**, 7308 (1995).

[52] D. J. Gross and F. Wilczek, Ultraviolet behavior of non-Abelian gauge theories, Phys. Rev. Lett. **30**, 1343 (1973).

[53] H. D. Politzer, Reliable perturbative results for strong interactions?, Phys. Rev. Lett. **30**, 1346 (1973).

[54] G. Ripka, *Dual Superconductor Models of Color Confinement* (Springer, 2005).

[55] A. Chodos, R. L. Jaffe, K. Johnson, C. B. Thorn, and V. F. Weisskopf, New extended model of hadrons, Phys. Rev. **D9**, 3471 (1974).

[56] A. Chodos, R. L. Jaffe, K. Johnson, and C. B. Thorn, Baryon structure in the bag theory, Phys. Rev. **D10**, 2599 (1974).

[57] T. DeGrand, R. L. Jaffe, K. Johnson, and J. Kiskis, Masses and other parameters of the light hadrons, Phys. Rev. **D12**, 2060 (1975).

[58] J. F. Donoghue and K. Johnson, The pion and an improved static bag model, Phys. Rev. **D21**, 1975 (1980).

[59] C. M. Bender and P. Hays, Zero-point energy of fields in a finite volume, Phys. Rev. **D14**, 2622 (1976).

[60] K. A. Milton, Toward finite zero-point energies in the bag model, Phys. Rev. **D27**, 439 (1983).

[61] A. Romeo, Gauge boson zero point energy in a spherical bag by the spectral zeta function method, Phys. Rev. **D53**, 3392 (1996).

[62] L. E. Oxman, N. F. Svaiter, and R. L. P. G. Amaral, Attractive Casimir effect in an infrared modified gluon bag model, Phys. Rev. **D72**, 125007 (2005), hep-th/0507195.

[63] D. B. Leinweber, Visualizations of quantum chromodynamics, `www.physics.adelaide.edu.au/~dleinweb/VisualQCD/Nobel/index.html`.

[64] F. Bissey *et al.*, Gluon flux-tube distribution and linear confinement in baryons, Phys. Rev. **D76**, 114512 (2007), hep-lat/0606016.

[65] J. Meixner and F. W. Schäfka, *Mathieusche Funcktionen and Sphäroidfunktionen* (Springer-Verlag, 1954).